bioRxiv preprint doi: https://doi.org/10.1101/395830; this version posted August 20, 2018. The copyright holder for this preprint (which was not certified by peer review) is the author/funder. All rights reserved. No reuse allowed without permission.

Human-specific *ARHGAP11B* induces hallmarks of neocortical expansion in developing ferret neocortex

Nereo Kalebic, Carlotta Gilardi, Mareike Albert, Takashi Namba, Katherine R. Long, Milos Kostic, Barbara Langen, Wieland B. Huttner*

Max Planck Institute of Molecular Cell Biology and Genetics, Pfotenhauerstraße 108, D-01307 Dresden, Germany

*Correspondence: huttner@mpi-cbg.de

bioRxiv preprint doi: https://doi.org/10.1101/395830; this version posted August 20, 2018. The copyright holder for this preprint (which was not certified by peer review) is the author/funder. All rights reserved. No reuse allowed without permission.

Abstract

The evolutionary increase in size and complexity of the primate neocortex is thought to underlie the higher cognitive abilities of humans. *ARHGAP11B* is a human-specific gene that, based on its expression pattern in fetal human neocortex and progenitor effects in embryonic mouse neocortex, has been proposed to have a key function in the evolutionary expansion of the neocortex. Here, we study the effects of *ARHGAP11B* expression in the developing neocortex of the gyrencephalic ferret. In contrast to its effects in mouse, ARHGAP11B markedly increases proliferative basal radial glia, a progenitor cell type thought to be instrumental for neocortical expansion, and results in extension of the neurogenic period and an increase in upper-layer neurons. As a consequence, the postnatal ferret neocortex exhibits an increased neuron density in the upper cortical layers and expands in the radial dimension. Thus, human-specific ARHGAP11B can elicit hallmarks of neocortical expansion in developing ferret neocortex.

bioRxiv preprint doi: https://doi.org/10.1101/395830; this version posted August 20, 2018. The copyright holder for this preprint (which was not certified by peer review) is the author/funder. All rights reserved. No reuse allowed without permission.

Introduction

The expansion of the neocortex during primate evolution is thought to constitute one important basis for the unparalleled cognitive abilities of humans. The size of the neocortex is mainly regulated by the proliferative potential of neural progenitor cells during cortical development and the length of the neurogenic period (Azevedo et al., 2009; Borrell and Götz, 2014; Dehay et al., 2015; Kaas, 2013; Kalebic et al., 2017; Krubitzer, 2007; Lui et al., 2011; Molnar et al., 2006; Rakic, 2009; Sousa et al., 2017; Wilsch-Bräuninger et al., 2016).

Two major classes of neural progenitors can be distinguished: apical progenitors (APs), whose cell bodies reside in the ventricular zone (VZ), and basal progenitors (BPs), whose cell bodies reside in the subventricular zone (SVZ). Whereas APs are highly proliferative in the neocortex of all mammalian species studied (Götz and Huttner, 2005; Rakic, 2003a), BPs are highly proliferative only in species with an expanded neocortex (Borrell and Götz, 2014; Florio and Huttner, 2014; Lui et al., 2011; Reillo et al., 2011). Specifically, a subtype of BPs, called basal (or outer) radial glia (bRG), are thought to play a key role in the evolutionary expansion of the neocortex (Borrell and Götz, 2014; Florio and Huttner, 2014; Lui et al., 2011). Importantly, in species with an expanded neocortex, such as primates or the ferret, the SVZ has been shown to be divided into two distinct histological zones: the inner and outer SVZ (ISVZ and OSVZ, respectively) (Dehay et al., 2015; Smart et al., 2002). The OSVZ is uniquely important for the evolutionary expansion of the neocortex, as proliferative bRG are particularly abundant in this zone (Betizeau et al., 2013; Fietz et al., 2010; Hansen et al., 2010; Poluch and Juliano, 2015; Reillo et al., 2011; Smart et al., 2002). Increased proliferative capacity of bRG results in an amplification of BP number and is accompanied by a prolonged phase of production of late-born neurons (Geschwind and Rakic, 2013; Otani et al., 2016; Rakic, 2009). As the mammalian

bioRxiv preprint doi: https://doi.org/10.1101/395830; this version posted August 20, 2018. The copyright holder for this preprint (which was not certified by peer review) is the author/funder. All rights reserved. No reuse allowed without permission.

cerebral cortex is generated in an inside-out fashion, these late-born neurons occupy the upper-most layers of the cortex (Lodato and Arlotta, 2015; Molnar et al., 2006; Molyneaux et al., 2007; Rakic, 1972, 2009; Sidman and Rakic, 1973). Thus, an increased generation of upper-layer neurons and increased thickness of the upper layers are also hallmarks of an expanded neocortex.

The evolutionary expansion of the neocortex is characteristically accompanied by an increase in the abundance of proliferative bRG, in the length of the neurogenic period, and in the relative proportion of upper-layer neurons within the cortical plate (Borrell and Götz, 2014; Dehay et al., 2015; Florio and Huttner, 2014; Geschwind and Rakic, 2013; Lui et al., 2011; Molnar et al., 2006; Sousa et al., 2017; Wilsch-Bräuninger et al., 2016). This is most obvious when comparing extant rodents, such as mouse, with primates, such as human. Carnivores, such as ferret, display intermediate features (Hutsler et al., 2005; Kawasaki, 2014). Specifically, ferrets exhibit a moderately gyrified neocortex and, during development, a pronounced OSVZ populated with proliferative bRG (Barnette et al., 2009; Borrell and Reillo, 2012; Fietz et al., 2010; Kawasaki, 2014; Kawasaki et al., 2013; Poluch and Juliano, 2015; Reillo et al., 2011; Sawada and Watanabe, 2012; Smart and McSherry, 1986a, b). In this context, it should be noted that in evolution, the split between the lineages leading to mouse and to human occurred a few million years later than that leading to ferret and human (Lewitus et al., 2014). This is consistent with the notion that the features associated with neocortex expansion in extant mammals occurred multiple times in the various lineages of the mammalian phylogenetic tree (Lewitus et al., 2014).

bioRxiv preprint doi: https://doi.org/10.1101/395830; this version posted August 20, 2018. The copyright holder for this preprint (which was not certified by peer review) is the author/funder. All rights reserved. No reuse allowed without permission.

In addition to the above-mentioned features associated with neocortex expansion in general, certain specific aspects of human neocortex expansion are thought to involve human-specific genomic changes. Recent transcriptomic studies established that certain previously identified human-specific genes (Bailey et al., 2002; Dennis and Eichler, 2016) are preferentially expressed in neural progenitor cells and have implicated these genes in human neocortex expansion (Fiddes et al., 2018; Florio et al., 2015; Florio et al., 2018; Florio et al., 2016; Suzuki et al., 2018). Among these genes, the one that showed the most specific expression in human bRG compared to neurons was *ARHGAP11B* (Florio et al., 2015). *ARHGAP11B* arose in evolution after the split of the human lineage from the chimpanzee lineage, as a product of a partial gene duplication of *ARHGAP11A*, a gene encoding a Rho GTPase activating protein (Dennis et al., 2017; Florio et al., 2015; Florio et al., 2016; Kagawa et al., 2013). Forced expression of *ARHGAP11B* in the embryonic mouse neocortex leads to an increase in BP proliferation and pool size (Florio et al., 2015). Here, we study the effects of forced expression of *ARHGAP11B* in the developing ferret neocortex, which already exhibits several features of an expanded neocortex, albeit at an inferior level compared to human.

bioRxiv preprint doi: https://doi.org/10.1101/395830; this version posted August 20, 2018. The copyright holder for this preprint (which was not certified by peer review) is the author/funder. All rights reserved. No reuse allowed without permission.

Results

We expressed ARHGAP11B in the ferret neocortex starting at embryonic day 33 (E33), when both the generation of upper-layer neurons and formation of the OSVZ start (Martinez-Martinez et al., 2016). Specifically, we performed *in utero* electroporation of ferrets (Kawasaki et al., 2012; Kawasaki et al., 2013) at E33 with a plasmid encoding *ARHGAP11B* under the constitutive CAG promoter or an empty vector as control. The analyses of electroporated embryos were performed at four different developmental stages: E37, E40/postnatal day (P) 0 , P10 and P16 (Figure 1 supplement 1A). To be able to visualize the electroporated area, we co-electroporated ARHGAP11B-expressing and control plasmids with vectors encoding fluorescent markers. For postnatal studies, to be able to distinguish the electroporated kits, the ARHGAP11B-expressing plasmid was co-electroporated with a GFP-encoding plasmid, and the control vector with an mCherry-encoding plasmid, or *vice versa*. For the sake of simplicity, we refer to both fluorescent markers as Fluorescent Protein (FP) from here onwards, and both FPs are depicted in green color in all figures.

We detected *ARHGAP11B* transcript by RT-qPCR at all the stages analyzed and only in ferret embryos/kits subjected to *ARHGAP11B in utero* electroporation (Figure 1 supplement 1B-D). Additionally, immunofluorescence at E37 demonstrated the specific presence of the ARHGAP11B protein in neural progenitors of such embryos (Figure 1 supplement 1E, F).

ARHGAP11B increases the abundance of BPs in the developing ferret neocortex

bioRxiv preprint doi: https://doi.org/10.1101/395830; this version posted August 20, 2018. The copyright holder for this preprint (which was not certified by peer review) is the author/funder. All rights reserved. No reuse allowed without permission.

We first examined the ability of ARHGAP11B to increase BP abundance in ferret. To this end, we immunostained E40/P0 ferret neocortex for PCNA, a marker of cycling cells, in order to identify progenitor cells (Figure 1A). We observed an increase in PCNA+ FP+ cells in the OSVZ of the ARHGAP11B-expressing embryos compared to control (Figure 1B, C). We next immunostained the E40/P0 ferret neocortex for phospho-vimentin (PhVim), a marker of mitotic cells (Figure 1D). Our analysis (Figure 1E, left) revealed a 3-fold increase in the abundance of mitotic cells between control and ARHGAP11B-expressing embryos. This increase was 6-fold for mitotic BPs, but only 2-fold (albeit not statistically significant) for mitotic APs (Figure 1E). A comparably large increase as was observed for BPs was detected when examining mitotic bRG, i.e. PhVim+ BPs exhibiting a PhVim+ process (Figure 1F, G), which accounted for 40% of all BPs (compare Figure 1E right, F). Taken together, these data indicate that ARHGAP11B markedly increases the abundance of BP, and specifically of bRG, when expressed in the embryonic ferret neocortex.

ARHGAP11B increases the proportion of Sox2-positive bRG that are Tbr2-negative

We next analyzed the ARHGAP11B-increased bRG in more detail. Proliferative neural progenitors, in particular apical radial glia (aRG) and bRG, characteristically express the transcription factor Sox2 (Pollen et al., 2015). We therefore immunostained E40/P0 ferret neocortex for Sox2 (Figure 2A) and detected a 40% increase in the proportion of Sox2+ FP+ cells in the germinal zones (GZs) (Figure 2B). This increase was exclusively due to an increase in BPs, as we observed a doubling of the proportion of Sox2+ FP+ cells in both the ISVZ and OSVZ, but no increase in the VZ, upon ARHGAP11B expression (Figure 2C).

bioRxiv preprint doi: https://doi.org/10.1101/395830; this version posted August 20, 2018. The copyright holder for this preprint (which was not certified by peer review) is the author/funder. All rights reserved. No reuse allowed without permission.

We then took advantage of a marker of neurogenic BPs, the transcription factor Tbr2 (Figure 2A) (Englund et al., 2005), which is expressed in mouse bRG, but not proliferative human bRG (Fietz et al., 2010; Florio et al., 2015; Hansen et al., 2010; Pollen et al., 2015). Upon expression of ARHGAP11B for 7 days, we observed a decrease in the proportion of Tbr2+ FP+ progenitors in all GZs, which was statistically significant for the VZ (Figure 2D, E).

In order to potentially obtain further cues as to the proliferative potential of the ARHGAP11B-increased bRG in the developing ferret neocortex, we focused our attention on progenitor cells that (i) exhibited a radial morphology, (ii) expressed Sox2, but (iii) lacked Tbr2 expression (Figure 2F). Upon ARHGAP11B expression, we observed, in the sum of the GZs, a 20% increase in the proportion of radial Sox2+ cells that were Tbr2– (Figure 2G). This was largely due to an increase in the proportion of these cells in the OSVZ (Figure 2H), where more than 90% were Tbr2–. These findings are consistent with the notion that the ARHGAP11B-increased radial Sox2+ Tbr2– cells in the OSVZ are bRG. Studies in fetal human neocortex have established that such cells in the OSVZ are highly proliferative ((Hansen et al., 2010; LaMonica et al., 2013) for reviews see (Florio and Huttner, 2014; Lui et al., 2011)). Hence, our finding that expression of ARHGAP11B in developing ferret neocortex results in a marked increase in the proportion of these cells suggests that this human-specific gene is sufficient to promote, in a gyrencephalic carnivore, the generation of bRG with increased proliferative potential.

ARHGAP11B expression in developing ferret neocortex results in an extended neurogenic period

bioRxiv preprint doi: https://doi.org/10.1101/395830; this version posted August 20, 2018. The copyright holder for this preprint (which was not certified by peer review) is the author/funder. All rights reserved. No reuse allowed without permission.

We investigated the potential consequences of the ARHGAP11B-elicited increase in the abundance of BPs, notably of Sox2+ Tbr2– bRG, for neurogenesis in the developing ferret neocortex. To this end, we immunostained E40/P0 ferret neocortex for Tbr1, a transcription factor which is a marker of deep-layer neurons (Kolk et al., 2006) (Figure 3 supplement 1A), and for Satb2, a transcriptional regulator which is expressed in neurons that establish callosal projections and that are highly enriched in the upper layers of the cortical plate (CP) (Alcamo et al., 2008; Britanova et al., 2008) (Figure 3A). The vast majority (>90%) of the FP+ neurons in the CP of both control and ARHGAP11B-expressing ferret neocortex were found to be Satb2+ (Figure 3 supplement 1B). This high percentage is consistent with our experimental approach in which we targeted the embryonic ferret neural progenitors by *in utero* electroporation at E33, i.e. the time when the generation of the upper-layer neurons starts (Jackson et al., 1989; Martinez-Martinez et al., 2016).

Analysis of the distribution of Satb2+ FP+ neurons at E40/P0 between the CP on the one hand side, and the GZs plus the intermediate zone (IZ) on the other hand side, revealed that around 60% of the neurons had reached the CP in both control and ARHGAP11B-expressing ferret neocortex (Figure 3B left). We next examined electroporated ferret neocortex at P10 (Figure 3 supplement 2; analysis confined to gyri), which is the stage when neuron production is completed and neuron migration is terminating in the motor and somatosensory areas (Jackson et al., 1989; Smart and McSherry, 1986a, b). Consistent with this, our analysis of the control brains revealed that more than 90% of the Satb2+ FP+ neurons had reached the CP (Figure 3B middle). In contrast, only 70% of the Satb2+ FP+ neurons were found in the CP of the ARHGAP11B-expressing neocortex (Figure 3B middle). However, at P16, nearly all Satb2+ FP+ neurons were found in the CP in both control and ARHGAP11B-expressing neocortex

bioRxiv preprint doi: https://doi.org/10.1101/395830; this version posted August 20, 2018. The copyright holder for this preprint (which was not certified by peer review) is the author/funder. All rights reserved. No reuse allowed without permission.

(Figure 3B right; again, analysis confined to gyri). These data suggested that upon ARHGAP11B expression, either neurons migrate more slowly to the CP, or the neurogenic period is extended.

To explore the latter scenario, we injected EdU into P5 ferret kits (i.e. 12 days after electroporation), which is the stage when neuronal progenitors undergo their very last neuron-generating cell divisions in the motor and somatosensory areas of the neocortex (Jackson et al., 1989; Smart and McSherry, 1986a, b). Analysis 11 days after EdU injection, at P16 (Figure 3C), revealed a 4-fold increase in the proportion of FP+ cells that were EdU+, in neocortical gyri of ARHGAP11B-expressing kits compared to control (Figure 3D). This was consistent with a prolonged, and hence increased, production of cells in ARHGAP11B-expressing kits, which in turn would be in line with the above described finding that ARHGAP11B increases the abundance of proliferative bRG. Importantly, among the EdU+ FP+ cells of the ARHGAP11B-expressing neocortex, 20% were Satb2+ neurons (Figure 3C' and E). In contrast, we did not detect a single Satb2+ EdU+ FP+ neuron in any of the control neocortices (Figure 3E). Collectively, these data indicate that neurogenesis in ARHGAP11B-expressing ferret neocortex continues longer than in control neocortex.

ARHGAP11B expression in developing ferret neocortex results in a greater abundance of upper-layer neurons

In light of the extension of the neurogenic period upon ARHGAP11B expression, we examined a potential increase in the abundance of the last-born neurons, that is, the upper-layer neurons. To this end, we first performed Nissl staining of the P16 ferret neocortex to visualize

bioRxiv preprint doi: https://doi.org/10.1101/395830; this version posted August 20, 2018. The copyright holder for this preprint (which was not certified by peer review) is the author/funder. All rights reserved. No reuse allowed without permission.

all neurons and the various layers of the CP, and immunostaining for Satb2, which is expressed in the majority of upper-layer neurons (Alcamo et al., 2008; Britanova et al., 2008; Lodato and Arlotta, 2015) (Figure 4A). These analyses, carried out on gyri, revealed (i) an increase in the abundance of FP+ cells in the CP (Figure 4 supplement 1A), and (ii) an alteration in the distribution of the FP+ cells between layers II-VI of the CP, with a greater proportion of cells in layers II-IV (Figure 4 supplement 1B), in the ARHGAP11B-expressing neocortex compared to control. A similar abundance increase (Figure 4 supplement 1C) and altered distribution (Figure 4B) were observed for Satb2+ FP+ neurons. Furthermore, the proportion of FP+ cells in the CP that were Satb2+ neurons was increased upon ARHGAP11B expression (Figure 4C).

We sought to corroborate these data by immunostaining the P16 ferret neocortex for Brn2 (Pou3f2, Figure 4 supplement 2A), a transcription factor considered to be a marker of layer II and III neurons (Dominguez et al., 2013; McEvilly et al., 2002; Sugitani et al., 2002). Quantification of Brn2+ FP+ cells in layers II and III of gyri revealed a marked increase in the abundance of these cells (Figure 4 supplement 2B) and in the proportion of FP+ cells that were Brn2+ neurons (Figure 4D), in ARHGAP11B-expressing kits compared to control. Of note, the effects of ARHGAP11B expression on the Brn2+ neurons were of a greater degree than those on the Satb2+ neurons (compare Figure 4 supplement 2B with Figure 4 supplement 1C; Figure 4, panel D with panel C), in line with the notion that Brn2 exhibits a greater specificity for layer II and III neurons than Satb2 (Dominguez et al., 2013; Sugitani et al., 2002). Taken together, our data indicate that the extension of the neurogenic period upon ARHGAP11B expression in the developing ferret neocortex is accompanied by an increase in the abundance of layer II and III neurons.

bioRxiv preprint doi: https://doi.org/10.1101/395830; this version posted August 20, 2018. The copyright holder for this preprint (which was not certified by peer review) is the author/funder. All rights reserved. No reuse allowed without permission.

ARHGAP11B expression in developing ferret neocortex leads to its radial expansion

Finally, we explored whether the ARHGAP11B-elicited increase in the abundance of BPs, notably of proliferative bRG, resulting in an extended neurogenic period and in an increased abundance of upper-layer neurons, had any consequences for the size and morphology of the ferret neocortex. To this end, we analyzed the neocortex at P16 (Figure 4 supplement 3A-C), the developmental stage when cortical folds have already formed in the ferret (Barnette et al., 2009; Fernandez et al., 2016; Matsumoto et al., 2017; Sawada and Watanabe, 2012; Shinmyo et al., 2017), and quantified a set of morphological parameters (Figure 4 supplement 3D), each on two coronal sections located slightly rostrally (Figure 4 supplement 3B and C, position 1) and slightly caudally (Figure 4 supplement 3B and D, position 2), respectively, to a middle position along the rostro-caudal axis. This revealed no significant differences between control and ARHGAP11B-expressing kits with regard to brain mass (Figure 4 supplement 3E) and gross neocortex morphology, including the gyrification index of the electroporated area (referred to as local GI), the size of the posterior sigmoid gyrus, lateral gyrus and coronal gyrus, and the depth and thickness of the cruciate sulcus, suprasylvian sulcus and lateral sulcus (Figure 4 supplement 3F-I).

However, we did detect an increase, upon ARHGAP11B expression, in the thickness of the three gyri analyzed (Figure 4E). We therefore investigated the underlying cause of this thickness increase and, considering the increased abundance of upper-layer neurons upon ARHGAP11B expression (Figure 4 supplement 1C, Figure 4 supplement 2B), measured the thickness of CP layers II-IV in the gyri of control and ARHGAP11B-expressing ferret neocortex at P16. This revealed a 100-µm increase in the thickness of these upper layers in ARHGAP11B-

bioRxiv preprint doi: https://doi.org/10.1101/395830; this version posted August 20, 2018. The copyright holder for this preprint (which was not certified by peer review) is the author/funder. All rights reserved. No reuse allowed without permission.

256 expressing neocortex compared to control (Figure 4F, note also the thicker layer II in Figure
257 4A and Figure 4 supplement 3K). Hence, ARHGAP11B is sufficient to promote neocortex
258 expansion in ferret in the radial dimension.
259
260 We then explored whether ARHGAP11B would also be able to promote neocortex expansion
261 in ferret in the tangential dimension. Here, we exploited the previous findings that during the
262 first week of the ferret postnatal neocortex development, migrating neurons change their
263 migration mode from radial to tangential, which results in an increased lateral dispersion of
264 the late-born neurons (Gertz and Kriegstein, 2015; Reillo et al., 2011; Smart and McSherry,
265 1986a, b). In line with this, the abundance of FP+ cells per 200 µm-wide field of cortical wall
266 decreased about 3-fold from E40/P0 to P16 (Figure 4 supplement 3J). Yet, the increase in FP+
267 cells per field of cortical wall due to ARHGAP11B expression was not only observed at P16,
268 confirming the above described analysis of FP+ cell numbers in the CP (Figure 4 supplement
269 1A), but was already detected at E40/P0 (Figure 4 supplement 3J). The decrease in FP+ cell
270 abundance per 200 µm-wide field of cortical wall from E40/P0 to P16 (Figure 4 supplement
271 3J) was not accompanied by an increase in cell death (Figure 4 supplement 4). Rather, this
272 decrease reflected an increase in the lateral spread of the progeny of the targeted cells, as
273 evidenced by the ARHGAP11B-elicited increase in the lateral length of the area harbouring
274 FP+ cells that was observed at P16, but not at E40/P0 (Figure 4G, H). Hence, ARHGAP11B is
275 sufficient to affect neocortex development in ferret also in the tangential dimension.
276
277 However, given that ARHGAP11B expression in the developing ferret neocortex increased the
278 lateral length of the area harbouring FP+ cells but did not increase gyrus size, we explored
279 whether this discrepancy could be resolved by ARHGAP11B expression increasing cell density,

bioRxiv preprint doi: https://doi.org/10.1101/395830; this version posted August 20, 2018. The copyright holder for this preprint (which was not certified by peer review) is the author/funder. All rights reserved. No reuse allowed without permission.

specifically in the upper layers of the CP where most of the ARHGAP11B-increased neurons resided. Indeed, our analysis revealed an increase in cell density in layers III and IV at P16, but not in layer II, which in general exhibited the highest cell density (Figure 4 supplement 3K, L). Taken together, these data indicate that the ARHGAP11B-promoted increase in upper-layer neurons, which resulted in their greater lateral spread, led to a higher cell density in those upper layers that were able to accommodate additional neurons, rather than to an increased gyrus size.

ARHGAP11B induces the appearance of astrocytes from the targeted progenitors in the developing ferret neocortex

Neocortex expansion involves not only an increase in the number of neurons, but also of glial cells. Although we on purpose performed *in utero* electroporation of the ferret neocortex at E33 in order to target OSVZ progenitors generating upper-layer neurons (Jackson et al., 1989; Martinez-Martinez et al., 2016), and therefore would expect only a small proportion of the FP+ cells to be glial cells, we nonetheless examined the possible occurrence of GFAP+ and S100ß+ cells (as indicators of an astrocytic lineage (Reillo et al., 2011; Voigt, 1989)) and of Olig2+ cells (as an indicator of an oligodendrocytic lineage (Mo and Zecevic, 2009; Voigt, 1989)) among the FP+ progeny of the targeted cells. An additional reason to examine astrocytes was that radial glial progenitor cells at later stages of human, monkey and ferret neocortex development are known to differentiate into astrocytic progenitors which then give rise to post-mitotic astrocytic cells (Rakic, 1978, 2003b; Reillo et al., 2011; Voigt, 1989).

bioRxiv preprint doi: https://doi.org/10.1101/395830; this version posted August 20, 2018. The copyright holder for this preprint (which was not certified by peer review) is the author/funder. All rights reserved. No reuse allowed without permission.

303 Upon immunostaining of the P16 ferret neocortex for GFAP (Figure 4 supplement 5A, B) and
304 Olig2 (Figure 4 supplement 5E), no FP+ cells in the CP of control neocortex that were GFAP+
305 or Olig2+ could be detected. In contrast, while we still did not detect any Olig2+ FP+ cells in
306 the CP of ARHGAP11B-expressing neocortex, about 3% of the CP FP+ cells were GFAP+ (Figure
307 4 supplement 5C). Given that ARHGAP11B expression increases the pool size of FP+ cells
308 (Figure 4 supplement 1A, Figure 4 supplement 3J), this translates into an ARHGAP11B-induced
309 appearance of GFAP+ FP+ cells in the CP. All of these GFAP+ FP+ cells were Ki67– (data not
310 shown) and hence post-mitotic astrocytes. To corroborate these data, we performed
311 immunostaining of the P16 ferret neocortex for another astrocyte marker, S100ß (Lopez-
312 Hidalgo et al., 2016), and readily identified FP+ S100ß+ astrocytes upon ARHGAP11B
313 expression. These data are consistent with at least two scenarios related to the increased
314 abundance of proliferative bRG upon ARHGAP11B expression. Either this increase results not
315 only in an extension of the neurogenic period but also in the initiation of astrogenesis. Or the
316 greater bRG pool size gives rise to a detectable level of astrocytic cells once the bRG
317 differentiate along the astrocytic lineage (Rakic, 2003b; Reillo et al., 2011; Voigt, 1989).
318

bioRxiv preprint doi: https://doi.org/10.1101/395830; this version posted August 20, 2018. The copyright holder for this preprint (which was not certified by peer review) is the author/funder. All rights reserved. No reuse allowed without permission.

Discussion

We have shown that expression of a single human-specific gene, *ARHGAP11B*, which has been implicated in the evolutionary expansion of the human neocortex (Florio et al., 2015; Florio et al., 2016), is sufficient to elicit features in the developing ferret neocortex that are characteristically associated with a further expanded neocortex such as human. These features include (i) an increase in the pool size of proliferative BPs, notably proliferative bRG; (ii) a lengthening of the neurogenic period; (iii) an increased generation of neurons, in particular of upper-layer neurons; and (iv) an increase in the size of the CP that harbours these additional neurons, reflected by the greater thickness of its upper layers and the larger lateral area where these neurons are found.

Increase in proliferative bRG. The present effects of ARHGAP11B on BPs in developing ferret neocortex are substantially greater than, and significantly different from, those previously observed upon transient *ARHGAP11B* expression in embryonic mouse neocortex (Florio et al., 2015), with regard to BP quantity and quality. As to quantity, in embryonic mouse neocortex, *ARHGAP11B* expression resulted in a doubling and tripling of the pool size of total BPs and BPs in mitosis, respectively (Florio et al., 2015), whereas in embryonic ferret neocortex, *ARHGAP11B* expression led to a 3.5-fold and 6-fold increase in the pool size of total BPs and BPs in mitosis (notably mitotic bRG), respectively (for a data summary, see Supplemental Table 1). The greater effect of *ARHGAP11B* expression on mitotic BP abundance than total BP abundance, in both embryonic mouse and ferret neocortex, indicates that *ARHGAP11B* expression increases the proportion of the total duration of the BP cell cycle that is used for M-phase. This in turn would be consistent with ARHGAP11B promoting, in embryonic ferret neocortex, the proliferative rather than neurogenic mode of bRG division. This notion would

bioRxiv preprint doi: https://doi.org/10.1101/395830; this version posted August 20, 2018. The copyright holder for this preprint (which was not certified by peer review) is the author/funder. All rights reserved. No reuse allowed without permission.

be in line with the previous findings that both, cortical progenitors in embryonic mouse neocortex (Arai et al., 2011) and radial glial progenitors in postnatal ferret neocortex (Turrero Garcia et al., 2015), which are not yet committed to neurogenesis spend a greater proportion of their total cell cycle in M-phase than those committed to neurogenesis.

As to BP quality, mouse bRG have been shown to undergo mostly neurogenic cell divisions and to display a limited proliferative capacity (Shitamukai et al., 2011; Wang et al., 2011; Wong et al., 2015). In contrast, human bRG are known to be highly proliferative, which is thought to be one of the key factors contributing to the evolutionary expansion of the human neocortex (Fietz et al., 2010; Florio and Huttner, 2014; Hansen et al., 2010; Lui et al., 2011). The proliferative capacity of bRG in other mammalian species that have been studied appears to follow the general rule that highly proliferative bRG are more often found in species with an expanded neocortex (Betizeau et al., 2013; Reillo et al., 2011). Hence, the ARHGAP11B-promoted increase in the number of proliferative (Sox2+ Tbr2–) bRG in the developing ferret neocortex fulfills a key requirement for further neocortex expansion.

In this context, it should be emphasized that those of the human-specific genes (Dennis and Eichler, 2016) that have been shown to be preferentially expressed in cortical progenitor cells (Florio et al., 2018) and that have been ectopically expressed in embryonic mouse neocortex, i.e. *ARHGAP11B* (Florio et al., 2015) and *NOTCH2NL* (Fiddes et al., 2018; Florio et al., 2018; Suzuki et al., 2018), show an increase in BP proliferation that mostly involves basal intermediate progenitors. To the best of our knowledge, our study provides first evidence of a human-specific gene increasing the number of proliferative bRG in a gyrencephalic neocortex. As bRG are considered to be instrumental for the evolutionary expansion of

bioRxiv preprint doi: https://doi.org/10.1101/395830; this version posted August 20, 2018. The copyright holder for this preprint (which was not certified by peer review) is the author/funder. All rights reserved. No reuse allowed without permission.

neocortex, this suggests that the ferret likely is a model system superior to mouse for studying the role of human-specific genes in neocortex development.

INCREASE IN UPPER-LAYER NEURONS. An increase in the upper layers is a fundamental characteristic of neocortex expansion (Fame et al., 2011; Hutsler et al., 2005; Molnar et al., 2006; Tarabykin et al., 2001). Layers II-IV are evolutionarily the most novel and mammalian-specific layers (Molnar et al., 2006). Layers II and III, in particular, underwent disproportional expansion during primate evolution. As the layers II-III neurons are the last-born neurons, an increase in the length of the neurogenic period might result in an increase in the number of late-born neurons. In fact, it has been proposed that the length of the neurogenic period may be a contributing factor in explaining the evolutionary increase in neocortex size and neuron number between humans and other great apes (Lewitus et al., 2014). Consistent with this, we observed a prolonged generation of late-born neurons, increased thickness of layers II-IV, and a marked increase in Satb2+ (3.3-fold) and, in particular, Brn2+ (5.6-fold) neurons in the upper layers of the CP, upon *ARHGAP11B* expression (for a data summary, see Supplemental Table 1). Thus, also with regard to the key product generated by cortical progenitor cells, i.e. the neurons, ARHGAP11B is sufficient to promote another feature in the developing ferret neocortex that would be consistent with further neocortex expansion.

In this context, Satb2+ neurons are of special interest, as Satb2 is essential for establishing callosal projections to the contralateral hemisphere (Alcamo et al., 2008; Britanova et al., 2008). Callosal projection neurons are considered to play a key role in the high-level associative connectivity, thus contributing significantly to human cognitive abilities, with their impairment causing cognition-related pathologies (Fame et al., 2011). Given that the

bioRxiv preprint doi: https://doi.org/10.1101/395830; this version posted August 20, 2018. The copyright holder for this preprint (which was not certified by peer review) is the author/funder. All rights reserved. No reuse allowed without permission.

evolutionary increase in neocortex size is accompanied by an increase in callosal projection neurons, our data show that ARHGAP11B elicits yet another, specific feature in the developing ferret neocortex associated with further neocortex expansion.

NEOCORTEX EXPANSION VS. INCREASED CP THICKNESS AND LATERAL AREA. A hallmark of neocortex expansion is neocortical folding (Borrell, 2018; Borrell and Götz, 2014; Kroenke and Bayly, 2018). Transient expression of *ARHGAP11B* in the embryonic mouse neocortex induced cortical folding in about half of the cases in this normally lissencephalic rodent (Florio et al., 2015). However, expression of ARHGAP11B in the developing ferret neocortex did not significantly increase the GI, gyrus size, or sulcus depth and thickness in this moderately gyrencephalic carnivore. The major morphological signs of neocortical expansion upon *ARHGAP11B* expression in developing ferret neocortex that we could detect were (i) an increased gyrus thickness, which reflected the already discussed increase in upper-layer thickness due to the increase in upper-layer neurons, and (ii) a larger lateral area of the CP where these neurons were found. The latter phenotype, however, did not result in an increase in gyrus size.

The reason why the increased upper-layer neurons generated upon *ARHGAP11B* expression – although increasing their final destination CP area in the tangential dimension – did not cause an increase in gyrus width, was that these neurons added themselves to the neurons already existing in the control condition, thereby increasing neuronal cell density in the upper layers. Analysis of cortical neuron density as a function of cortical neuron number across carnivores has revealed that neuron density tends to decrease with increasing neuron number (Herculano-Houzel et al., 2015; Jardim-Messeder et al., 2017; Lewitus et al., 2012). This trend

bioRxiv preprint doi: https://doi.org/10.1101/395830; this version posted August 20, 2018. The copyright holder for this preprint (which was not certified by peer review) is the author/funder. All rights reserved. No reuse allowed without permission.

415 is much less prominent in primates, which in general exhibit a greater cortical neuron density
416 per cortical neuron number than carnivores. Thus, the increase in upper-layer neuron density
417 upon increasing upper-layer neuron number by the human-specific *ARHGAP11B* can be
418 regarded as a form of "primatization" of the ferret neocortex.
419
420 In this context, it is interesting to note that neocortical neuron density across carnivores shows
421 a much greater range of variation than that across primates. We therefore hypothesize that
422 the ferret neocortex is plastic enough to accommodate additional neurons, without having to
423 increase neocortex size or folding. A corollary of this notion with regard to ARHGAP11B is that
424 its primary function is to increase the proliferation and thus pool size of BPs, notably of bRG,
425 which results in a lengthening of the neurogenic period and an increased generation of
426 neurons, in particular of upper-layer neurons. Whether this leads to an increase in cortical
427 folding as an indicator of neocortex expansion, as found in ARHGAP11B-expressing mouse
428 embryos (Florio et al., 2015), or to an increase in cortical neuron density, as observed in the
429 present study with ARHGAP11B-expressing ferret kits, appears to reflect more the inherent
430 properties of the mammalian order under study how to deal with an increase in cortical
431 neuron number, rather than the primary function of ARHGAP11B.
432

bioRxiv preprint doi: https://doi.org/10.1101/395830; this version posted August 20, 2018. The copyright holder for this preprint (which was not certified by peer review) is the author/funder. All rights reserved. No reuse allowed without permission.

433 **Author contributions**:

434

435 Conceptualization, N.K., W.B.H.; Formal Analysis, N.K.; Investigation, N.K., C.G., M.A.;
436 Methodology, N.K., C.G., K.R.L., M.K., B.L.; Visualization, N.K., C.G.; Resources, T.N.; Writing -
437 Original draft, N.K.; Writing - Review & editing, N.K., W.B.H.; Supervision, W.B.H.; Project
438 Administration and Funding Acquisition, W.B.H.. All authors gave input on the manuscript.

439

440 **Acknowledgements**:

441 We are grateful to the Services and Facilities of the Max Planck Institute of Molecular Cell
442 Biology and Genetics for the outstanding support provided, notably J. Helppi and his team of
443 the Biomedical services (BMS) for the excellent husbandry of ferrets, J. Peychl and his team of
444 the Light Microscopy Facility and P.Keller and his team of the Antibody Facility. We would like
445 to particularly thank Anke Münch-Wuttke for help with perfusion of ferret kits and Dr. Anna
446 Pfeffer for exceptional veterinary support. NK was supported by an EMBO long-term
447 fellowship (ALTF 861-2013). CG acknowledges support from the Erasmus+ traineeship
448 program and MA from the Christiane-Nüsslein-Volhard Foundation. WBH was supported by
449 grants from the DFG (SFB 655, A2), the ERC (250197) and ERA-NET NEURON (MicroKin).

450

451 **Declaration of interests**:

452 The authors declare no competing interests.

453

bioRxiv preprint doi: https://doi.org/10.1101/395830; this version posted August 20, 2018. The copyright holder for this preprint (which was not certified by peer review) is the author/funder. All rights reserved. No reuse allowed without permission.

Figure legends

Figure 1. ARHGAP11B increases the abundance of BPs in the developing ferret neocortex.

Ferret E33 neocortex was electroporated *in utero* with a plasmid encoding a fluorescent protein (FP) together with either a plasmid encoding ARHGAP11B or empty vector (Control), followed by analysis at E40/P0.

(A) Double immunofluorescence for FP (green) and PCNA (magenta), combined with DAPI staining (white). Images are single optical sections. Scale bars, 50 µm. Boxes (50 x 50 µm) indicate an FP+ BP in the OSVZ, shown at higher magnification on the right. Dashed lines indicate a cell body contour.

(B, C) Percentage of FP+ cells in the germinal zones (B, GZ) and in the VZ (C, left), ISVZ (C, center) and OSVZ (C, right) that are PCNA+ upon control (white) and ARHGAP11B (black) electroporations. Data are the mean of 3 experiments. Error bars indicate SD; n.s., not statistically significant; *, P <0.05, Student's *t*-test.

(D) Double immunofluorescence for FP (green) and phospho-vimentin (PhVim, magenta), combined with DAPI staining (white). Images are single optical sections. Scale bars, 50 µm. Vertical arrowheads, apical mitosis; horizontal arrowheads, basal mitosis.

(E) Quantification of total (left), apical (center) and basal (right) FP+ mitotic cells, as revealed by PhVim immunofluorescence, in a 200 µm-wide field of the cortical wall, upon control (white) and ARHGAP11B (black) electroporations. Data are the mean of 4 experiments. Error bars indicate SD; n.s., not statistically significant, *, P <0.05, Mann-Whitney *U*-test.

(F) Quantification of mitotic bRG (FP+ PhVim+ cell bodies in the SVZ that contain a PhVim+ process), in a 200 µm-wide field of cortical wall, upon control (white) and ARHGAP11B (black) electroporations. Data are the mean of 4 experiments. Error bars indicate SD; *, P <0.05, Mann-Whitney *U*-test.

(G) Mitotic bRG (single optical sections). Double immunofluorescence for FP (green) and phospho-vimentin (PhVim, magenta), combined with DAPI staining (white), upon electroporation of the plasmid encoding FP together with the plasmid encoding ARHGAP11B. Arrowheads, PhVim+ basal process of the mitotic bRG. Images are oriented with the apical side facing down and are 25 µm wide.

Figure 2. ARHGAP11B increases the proportion of Sox2-positive bRG that are Tbr2-negative

bioRxiv preprint doi: https://doi.org/10.1101/395830; this version posted August 20, 2018. The copyright holder for this preprint (which was not certified by peer review) is the author/funder. All rights reserved. No reuse allowed without permission.

Ferret E33 neocortex was electroporated *in utero* with a plasmid encoding FP together with either a plasmid encoding ARHGAP11B or empty vector (Control), followed by triple immunofluorescence for FP (green), Sox2 (yellow) and Tbr2 (magenta), combined with DAPI staining (white), at E40/P0.

(A) Overview of the electroporated areas (single optical sections). Scale bars, 50 µm.

(B, C) Percentage of FP+ cells in the germinal zones (B, GZ) and in the VZ (C, left), ISVZ (C, center) and OSVZ (C, right) that are Sox2+ upon control (white) and ARHGAP11B (black) electroporations.

(D, E) Percentage of FP+ cells in the germinal zones (D, GZ) and in the VZ (E, left), ISVZ (E, center) and OSVZ (E, right) that are Tbr2+ upon control (white) and ARHGAP11B (black) electroporations.

(F) Proliferative bRG (Sox2+ Tbr2– cell in the SVZ exhibiting radial morphology, single optical sections). Triple immunofluorescence for FP (green), Sox2 (yellow) and Tbr2 (magenta), combined with DAPI staining (white), upon electroporation of the plasmid encoding FP together with the plasmid encoding ARHGAP11B. Dashed lines, cell body. Images are oriented with the apical side facing down and are 25 µm wide.

(G, H) Percentage of Sox2+ FP+ cells exhibiting radial morphology in the germinal zones (G, GZ) and in the VZ (H, left), ISVZ (H, center) and OSVZ (H, right) that are Tbr2– upon control (white) and ARHGAP11B (black) electroporations.

(B-E, G, H) Data are the mean of 4 experiments. Error bars indicate SD; n.s., not statistically significant; ***, P<0.001; **, P <0.01; *, P <0.05, Student's *t*-test.

Figure 3. ARHGAP11B expression in developing ferret neocortex results in an extended neurogenic period

Ferret E33 neocortex was electroporated *in utero* with a plasmid encoding FP, together with either a plasmid encoding ARHGAP11B or empty vector (Control), followed by analysis at E40/P0 (A, B left), P10 (B center) and P16 (B right, C-E).

(A) Double immunofluorescence for FP (green) and Satb2 (magenta), combined with DAPI staining (white), of the E40/P0 ferret neocortex. The immunofluorescence of the same cryosection for Tbr1 is shown in Figure 3 supplement 1A. Images are single optical sections. Scale bars, 50 µm.

bioRxiv preprint doi: https://doi.org/10.1101/395830; this version posted August 20, 2018. The copyright holder for this preprint (which was not certified by peer review) is the author/funder. All rights reserved. No reuse allowed without permission.

(B) Distribution of Satb2+ FP+ neurons at E40/P0 (left), P10 (center) and P16 (right), between the cortical plate (CP, green) and germinal zones plus intermediate zone (GZ+IZ, yellow), upon control (Con, left) and ARHGAP11B (11B, right) electroporations. Data are the mean of 3 (P0 and P10) or 4 (P16) experiments. Error bars indicate SD; **, P <0.01; n.s., not statistically significant, two-way ANOVA with Bonferroni post-hoc tests (P10, Control CP vs. ARHGAP11B CP, P=0.0015).

(C) Triple (immuno)fluorescence for FP (green), Satb2 (magenta) and EdU (yellow), combined with DAPI staining (white), of the P16 ferret neocortex, upon EdU injection at P5. Images are single optical sections. Scale bars, 1 mm. (C') Higher magnification of a FP+ Satb2+ EdU+ neuron upon electroporation of the plasmid encoding FP together with the plasmid encoding ARHGAP11B. Dashed lines, cell body. Images (single optical sections) are oriented with the apical side facing down and are 50 µm wide.

(D) Percentage of FP+ cells that are EdU+ upon control (white) and ARHGAP11B (black) electroporations.

(E) Percentage of EdU+ FP+ cells that are Satb2+ upon control (white) and ARHGAP11B (black) electroporations.

(D, E) Data are the mean of 3 experiments. Error bars indicate SD; ***, P <0.001; *, P <0.05, Student's *t*-test.

Figure 4. ARHGAP11B expression results in a greater abundance of upper-layer neurons and expansion of the developing ferret neocortex

Ferret E33 neocortex was electroporated *in utero* with a plasmid encoding FP, together with either a plasmid encoding ARHGAP11B or empty vector (Control), followed by analysis at E40/P0 (G, left) or P16 (all other panels).

(A) Double immunofluorescence for FP (green) and Satb2 (magenta), combined with DAPI (white) and Nissl (yellow) staining, of the CP (single optical sections). Neuronal layers are marked on the left. Arrowheads, increased thickness of layer II upon ARHGAP11B expression. Scale bars, 200 µm.

(B) Distribution of Satb2+ FP+ neurons between the neuronal layers upon control (Con, left) and ARHGAP11B (11B, right) electroporations. Data are the mean of 6 experiments. Error bars indicate SD; ***, P <0.001, two-way ANOVA with Bonferroni post-hoc tests (Layer V, Control vs. ARHGAP11B, P <0.0001; Layer III, Control vs. ARHGAP11B, P=0.0073)

bioRxiv preprint doi: https://doi.org/10.1101/395830; this version posted August 20, 2018. The copyright holder for this preprint (which was not certified by peer review) is the author/funder. All rights reserved. No reuse allowed without permission.

549 (C) Percentage of FP+ cells in the CP that are Satb2+, upon control (white) and ARHGAP11B
550 (black) electroporations. Data are the mean of 6 experiments. Error bars indicate SD; ***, P
551 <0.001, Student's *t*-test.
552 (D) Percentage of FP+ cells in layers II+III that are Brn2+, upon control (white) and ARHGAP11B
553 (black) electroporations. Data are the mean of 5 experiments. Error bars indicate SD; *, P
554 <0.05, Student's *t*-test.
555 (E) Quantification of the gyrus thickness of control (Con) and ARHGAP11B-expressing (11B)
556 ferret neocortex. Measurements were performed as described in Figure 4 supplement 3. All
557 data are expressed as ratio between electroporated hemisphere (IUE) and non-electroporated
558 contralateral hemisphere (non-IUE). Data are the mean (red lines) of 20 gyri per condition
559 from 6 neocortices per condition. Error bars indicate SD; *, P <0.05, Student's *t*-test.
560 (F) Quantification of layers II-IV thickness, upon control (Con, white) and ARHGAP11B (11B,
561 black) electroporations. Data are the mean of 6 experiments. Error bars indicate SD; *, P <0.05,
562 Student's *t*-test.
563 (G) Immunofluorescence for FP (green), combined with DAPI staining (white), of the areas
564 harbouring FP+ cells (single optical sections). Dashed lines, basal contour of the FP+ area.
565 Lateral length of the respective contour is indicated in the bottom right corner. Note that the
566 images and the countours depict only the areas with a high abundance of FP+ cells, which is
567 distinct from the quantification shown in (G). Scale bars, 1 mm.
568 (H) Quantification of the lateral length of the entire areas harbouring FP+ cells, measured as
569 depicted in Figure 4 supplement 3D middle, at E40/P0 (left) and P16 (right), upon control (Con,
570 white) and ARHGAP11B (11B, black) electroporations. Data are the mean of 3 (E40/P0) and 6
571 (P16) experiments. Error bars indicate SD; **, P <0.01, Student's *t*-test.
572

bioRxiv preprint doi: https://doi.org/10.1101/395830; this version posted August 20, 2018. The copyright holder for this preprint (which was not certified by peer review) is the author/funder. All rights reserved. No reuse allowed without permission.

Supplemental figure legends

Figure 1 supplement 1. Forced expression of ARHGAP11B in the developing ferret neocortex.

(A) Scheme of ferret neocortex development and experimental approach. ARHGAP11B was expressed in developing ferret neocortex by *in utero* electroporation at E33, when the OSVZ begins to form. Analyses were performed at E37, E40/P0, P10 and P16. Analysis of cortical progenitors was performed at E40/P0, analysis of post-mitotic cells at E40/P0, P10 and P16, and analysis of brain size and neocortex morphology at P16.

(B-D) mRNA expression analysis by RT-qPCR at E37, P0, P10 and P16. RNA was isolated from cryosections of paraformaldehyde-fixed brain tissue following ferret *in utero* electroporation at E33. Expression of the housekeeping gene *Hprt1* (B, note the lack of signal in the absence of reverse transcriptase (–RT)) was used for normalization of *ARHGAP11B* expression detected with two different primer pairs (C, *ARHGAP11B_1*; D, *ARHGAP11B_2*). Two control (Con_1, Con_2; white) and two ARHGAP11B-electroporated (11B_1, 11B_2; black) embryos were analyzed at each stage, except for P0 when one control and one ARHGAP11B-electroporated embryo were analyzed. Error bars represent SD of three PCR amplifications.

(E, F) ARHGAP11B protein expression analysis by immunofluorescence. Ferret E33 neocortex was electroporated *in utero* with a plasmid encoding FP together with either a plasmid encoding ARHGAP11B or empty vector (Control), followed by analysis at E37.

(E) Triple immunofluorescence for FP (green), ARHGAB11B (11B, magenta) and Arhgap11a (11a, yellow), combined with DAPI staining (white). Arrows, an ARHGAP11B+ FP+ cell that is Arhgap11a–; arrowheads, an Arhgap11a+ cell that is FP– ARHGAP11B–. Note that the exposure of images of ARHGAP11B staining in the control neocortex was longer than in the ARHGAP11B-electroporated neocortex, in order to show the lack of a specific signal in the control, where only unspecific signal at blood vessels was detected (asterisks). Images are single optical sections. Scale bars, 50 µm.

(F) Triple immunofluorescence for FP (green), ARHGAB11B (11B, magenta) and Ki67 (yellow), combined with DAPI staining (white), upon electroporation of a plasmid encoding FP and a plasmid encoding ARHGAP11B. Images are single optical sections. Scale bar, 20 µm. Boxes (25 µm wide), indicating an ARHGAP11B-expressing BP (upper box) and an ARHGAP11B-expressing AP (lower box), are shown at higher magnification on the right. Dashed lines, cell bodies.

bioRxiv preprint doi: https://doi.org/10.1101/395830; this version posted August 20, 2018. The copyright holder for this preprint (which was not certified by peer review) is the author/funder. All rights reserved. No reuse allowed without permission.

Figure 3 supplement 1. Almost all neurons generated from ARHGAP11B-expressing progenitors are Satb2+.

Ferret E33 neocortex was electroporated *in utero* with a plasmid encoding FP together with either a plasmid encoding ARHGAP11B or empty vector (Control), followed by triple immunofluorescence for FP, Tbr1 and Satb2, combined with DAPI staining, at E40/P0.

(A) Overview of the electroporated areas showing the immunofluorescence for Tbr1 (yellow) and FP (green) and the DAPI staining (white) (single optical sections). Note that the DAPI staining and FP immunofluorescence images are the same as in Figure 3A; for Satb2 staining, see Figure 3A. Scale bars, 50 µm.

(B) Percentages of FP+ cells that are Satb2+ Tbr1– (blue), Satb2+ Tbr1+ (purple) and Satb2– Tbr1+ (yellow), upon control (left) and ARHGAP11B (right) electroporations. Data are the mean of 3 experiments. Error bars indicate SD.

Figure 3 supplement 2. FP and Satb2 immunostaining patterns of control and ARHGAP11B-expressing developing ferret neocortex at P10.

Ferret E33 neocortex was electroporated *in utero* with a plasmid encoding FP together with either a plasmid encoding ARHGAP11B or empty vector (Control), followed by double immunofluorescence for FP (green) and Satb2 (magenta), combined with DAPI staining (white), at P10. Images are maximum intensity projections of 5 optical sections. Scale bars, 1 mm.

Figure 4 supplement 1. ARHGAP11B expression results in a greater abundance of FP+ cells and FP+ Satb2+ neurons in the CP.

Ferret E33 neocortex was electroporated *in utero* with a plasmid encoding FP together with either a plasmid encoding ARHGAP11B or empty vector (Control), followed by analysis at P16.

(A, C) Quantification of FP+ cells (A) and Satb2+ FP+ cells (C) in a 200 µm-wide field in the CP, upon control (white) and ARHGAP11B (black) electroporations. Data are the mean of 6 experiments. Error bars indicate SD; **, P <0.01; *, P <0.05, Student's *t*-test.

(B) Distribution of FP+ cells between the neuronal layers upon control (Con, left) and ARHGAP11B (11B, right) electroporations. Data are the mean of 6 experiments. Error bars indicate SD; **, P <0.01, two-way ANOVA with Bonferroni post-hoc tests (Layer V, Control vs. ARHGAP11B, P=0.014).

bioRxiv preprint doi: https://doi.org/10.1101/395830; this version posted August 20, 2018. The copyright holder for this preprint (which was not certified by peer review) is the author/funder. All rights reserved. No reuse allowed without permission.

Figure 4 supplement 2. ARHGAP11B expression results in a greater abundance of FP+ Brn2+ neurons in cortical layers II and III.

Ferret E33 neocortex was electroporated *in utero* with a plasmid encoding FP together with either a plasmid encoding ARHGAP11B or empty vector (Control), followed by double immunofluorescence for FP and Brn2, combined with DAPI staining, at P16.

(A) Overview of the CP of the electroporated area showing the immunofluorescence for FP (green) and Brn2 (magenta) and the DAPI staining (white) (single optical sections). Layers II and III are indicated on the left. Scale bars, 100 µm. Boxes (50 x 50 µm) indicate a Brn2+ FP+ neuron in layer II, shown at higher magnification on the right. Dashed lines, cell body.

(B) Quantification of Brn2+ FP+ cells in a 200 µm-wide field in layers II+III (left), in layer II only (center) and in layer III only (right), upon control (white) and ARHGAP11B (black) electroporations. Data are the mean of 5 experiments. Error bars indicate SD; **, P <0.01; *, P <0.05, Student's *t*-test.

Figure 4 supplement 3. ARHGAP11B expression in developing ferret neocortex leads to its expansion.

Ferret E33 neocortex was electroporated *in utero* with a plasmid encoding FP together with either a plasmid encoding ARHGAP11B or empty vector (Control), followed by analysis at E40/P0 (K, left) or P16 (all other panels).

(A) Image of an electroporated brain, with the electroporated area in orange. R, rostral; C, caudal.

(B) Schematic representation of the P16 ferret brain (dorsal view). Lines 1 and 2 indicate the positions at which all the morphological measurements were performed. Position 1 is exemplified in (C) and position 2 in (D).

(C) Immunofluorescence for FP (green), combined with DAPI staining (white), of electroporated brains at position 1 (see B). Images are single optical sections. Scale bar, 1 mm.

(D) Graphical definition of the measured morphological parameters. Double immunofluorescence for FP (green) and GFAP (magenta), combined with DAPI staining (white), of electroporated brain at position 2 (see B). Image (shown three times) is a single optical section. Yellow lines indicate measured parameters. See also Methods section for details.

bioRxiv preprint doi: https://doi.org/10.1101/395830; this version posted August 20, 2018. The copyright holder for this preprint (which was not certified by peer review) is the author/funder. All rights reserved. No reuse allowed without permission.

(E) Quantification of the weight of the control (Con) and ARHGAP11B-expressing (11B) ferret brains. Data are the mean (red lines) of 7 (control) or 9 (ARHGAP11B) brains.

(F-I) Quantification of the indicated morphological parameters (see (D)), i.e. the gyrification index of the electroporated area (referred to as local GI) (F), gyrus size (G), sulcus depth (H) and sulcus thickness (I), of control (Con) and ARHGAP11B-expressing (11B) ferret neocortex. Measurements were performed at positions 1 and 2 (see (D)); for gyrus morphology, the posterior sigmoid gyrus (position 1), lateral gyrus (position 2) and the coronal gyrus (positions 1 and 2) were analyzed, yielding up to 4 data points; for sulcus morphology, the cruciate sulcus (position 1), lateral sulcus (position 2) and the suprasylvian sulcus (positions 1 and 2) were analyzed, also yielding up to 4 data points. Please refer to Sawada and Watanabe (2012) for the ferret gyri and sulci nomenclature. All data are expressed as ratio between electroporated hemisphere (IUE) and non-electroporated contra-lateral hemisphere (non-IUE).

(F-H) Data are the mean (red lines) of 6 neocortices per condition.

(I) Data are the mean (red lines) of 18 (control) and 19 (ARHGAP11B) sulci from 6 neocortices per condition.

(J) Quantification of the number of FP+ cells in a 200 µm-wide field of cortical wall at E40/P0 (left) and P16 (right), upon control (white) and ARHGAP11B (black) electroporations. Data are the mean of 6 experiments.

(K) Immunofluorescence for FP (green), combined with DAPI staining (white), of the indicated upper layers of the CP at position 2. Images are single optical sections. Scale bars, 20 µm.

(L) Quantification of cell density, as revealed by DAPI staining of nuclei, in 50 µm x 50 µm fields of layer II (left), layer III (center) and layer IV (right) of the CP, upon control (white) and ARHGAP11B (black) electroporations. Data are the mean (red lines) of 4 (control) and 5 (ARHGAP11B) experiments, with 3 fields per layer per experiment.

(E-J, L) Error bars indicate SD; ***, P<0.001; **, P <0.01; *, P <0.05; n.s., not statistically significant, Student's *t*-test.

Figure 4 supplement 4. ARHGAP11B expression in developing ferret neocortex does not lead to increased cell death.

Ferret E33 neocortex was electroporated *in utero* with a plasmid encoding FP together with either a plasmid encoding ARHGAP11B or empty vector (Control), followed by analysis at E40/P0 (A, F), P10 (B, C, F) and P16 (D, E, F).

bioRxiv preprint doi: https://doi.org/10.1101/395830; this version posted August 20, 2018. The copyright holder for this preprint (which was not certified by peer review) is the author/funder. All rights reserved. No reuse allowed without permission.

(A) Immunofluorescence for FP (green), combined with DAPI staining (white) and TUNEL (terminal deoxynucleotidyl transferase dUTP nick end labeling) staining (magenta), of the E40/P0 ferret neocortex. Image width, 200 µm.

(B) Double immunofluorescence for FP (green) and Caspase-3 (magenta), combined with DAPI staining (white), of the P10 ferret neocortex. Scale bar, 500 µm.

(C) Immunofluorescence for FP (green), combined with staining using fluorescently labeled annexin V (yellow) and DAPI staining (white), of the P10 ferret neocortex. TUNEL staining (magenta) is shown for the ARHGAP11B-expressing neocortex. Image width, 200 µm.

(D) Immunofluorescence for FP (green), combined with DAPI staining (white) and TUNEL staining (magenta), of the P16 ferret neocortex. Scale bar, 500 µm.

(E) Immunofluorescence for FP (green), combined with staining using fluorescently labeled annexin V (yellow) and DAPI staining (white), of the cortical plate of the P16 ferret neocortex. Scale bar, 300 µm.

(A-E) All images are single optical sections.

(F) Percentage of FP+ cells that are apoptotic. Note that at all stages analyzed and by all detection methods, ARHGAP11B-expressing neocortex does not show an increase in apoptosis. Data are the mean of at least two neocortices per condition.

Figure 4 supplement 5. ARHGAP11B induces the appearance of astrocytes from the targeted progenitors in the developing ferret neocortex.

Ferret E33 neocortex was electroporated *in utero* with a plasmid encoding FP together with either a plasmid encoding ARHGAP11B or empty vector (Control), followed by analysis at P16.

(A, B) Double immunofluorescence for FP (green) and GFAP (magenta), combined with DAPI staining (white), of the CP (A, single optical sections). Scale bars, 100 µm. (B) High magnification of an FP+ GFAP+ ARHGAP11B-expressing cell in the CP from a different experiment than (A). Arrows, cell body; arrowheads, cell processes. Image width, 36.7 µm.

(C) Percentage of FP+ cells in the CP that are GFAP+, upon control (white) and ARHGAP11B (black) electroporations. Data are the mean of 4 experiments. Error bars indicate SD; *, P <0.05, Student's *t*-test.

(D) Double immunofluorescence for FP (green) and S100ß (magenta), combined with DAPI staining (white), of the CP (single optical sections). Scale bars, 100 µm. Boxes (75.5 µm wide)

bioRxiv preprint doi: https://doi.org/10.1101/395830; this version posted August 20, 2018. The copyright holder for this preprint (which was not certified by peer review) is the author/funder. All rights reserved. No reuse allowed without permission.

indicate an FP+ S100ß+ cell in the CP, shown at higher magnification in the bottom images. Arrows, cell body; arrowheads, cell process.

(E) Double immunofluorescence for FP (green) and Olig2 (magenta), combined with DAPI staining (white), of the CP (single optical sections). Scale bars, 100 µm. Boxes (52 x 52 µm) indicate an FP+ Olig2– cell in the CP, shown at higher magnification on the right. Note that no cells were found to be FP+ Olig2+.

Supplemental Table 1. Overview of the effects of ARHGAP11B expression on neural progenitor cells and upper-layer neurons in developing ferret neocortex.

Data taken from the indicated figure panels were used for the calculations shown. For the calculations pertaining to upper-layer neurons, it is assumed that the ARHGAP11B-induced increase in the lateral length of the FP+ area in the rostro-caudal dimension is equal to that in the medio-lateral dimension (1.25-fold).

bioRxiv preprint doi: https://doi.org/10.1101/395830; this version posted August 20, 2018. The copyright holder for this preprint (which was not certified by peer review) is the author/funder. All rights reserved. No reuse allowed without permission.

MATERIALS AND METHODS

KEY RESOURCES TABLE

REAGENT or	SOURCE	IDENTIFIER	ADDITIONAL INFORMATION
Antibodies			
Goat anti-Sox2	R+D Systems	AF2018, RRID:AB_355110	1:200
Goat anti-Sox2	Santa Cruz Biotechnology	sc-17320 RRID:AB_2286684	1:200
Rabbit anti-Tbr2	Abcam	ab23345, RRID:AB_778267	1:250
Mouse anti-PCNA	Millipore	CBL407, RRID:AB_93501	1:200
Mouse anti-PhVim	Abcam	ab22651, RRID:AB_447222	1:200
Mouse anti-Satb2	Abcam	ab51502, RRID:AB_882455	1:200
Rabbit anti-Tbr1	Abcam	ab31940, RRID:AB_2200219	1:200
Rabbit anti-Brn2	Proteintech	18998-1-AP, RRID:AB_10597389	1:100
Rabbit anti-Olig2	Millipore	ab9610, RRID:AB_570666	1:500
Rabbit anti-GFAP	Dako	Z0334, RRID:AB_10013382	1:1000
Rabbit anti-S100ß	Abcam	ab868, RRID:AB_306716	1:200
Rabbit anti-active Caspase 3	Abcam	ab2302 RRID:AB_302962	1:200
Mouse anti-ARHGAP11B	MPI-CBG	N.A.	1:100
Rabbit anti-Arhgap11A	Abcam	ab113261, RRID:AB_10866587	1:500
Chicken anti-GFP	Aves labs	GFP1020, RRID:AB_10000240	1:1000
Goat anti-GFP	MPI-CBG	N.A.	1:1000
Rat anti-RFP	ChromoTek	5F8, RRID:AB_2336064	1:500
Rabbit anti-RFP	Rockland antibodies	600-401-379, RRID:AB_2209751	1:1000
Goat anti-Chicken Alexa Fluor 488	ThermoFisher Scientific	A11039, RRID:AB_142924	1:500
Donkey anti-Goat Alexa Fluor 488	ThermoFisher Scientific	A11055, RRID:AB_2534102	1:500
Donkey anti-Goat Alexa Fluor 555	ThermoFisher Scientific	A21432, RRID:AB_2535853	1:500
Donkey anti-Goat Alexa Fluor 647	ThermoFisher Scientific	A21447, RRID:AB_141844	1:500
Donkey anti-Rabbit Alexa Fluor 488	ThermoFisher Scientific	A21206, RRID:AB_141708	1:500
Donkey anti-Rabbit Alexa Fluor 555	ThermoFisher Scientific	A31572, RRID:AB_162543	1:500
Donkey anti-Rabbit Alexa Fluor 647	ThermoFisher Scientific	A-31573, RRID:AB_2536183	1:500 or 1:1000
Donkey anti-Mouse Alexa Fluor 488	ThermoFisher Scientific	A-21202, RRID:AB_141607	1:500 or `1:1000
Donkey anti-Mouse Alexa Fluor 555	ThermoFisher Scientific	A31570, RRID:AB_2536180	1:500

bioRxiv preprint doi: https://doi.org/10.1101/395830; this version posted August 20, 2018. The copyright holder for this preprint (which was not certified by peer review) is the author/funder. All rights reserved. No reuse allowed without permission.

Donkey anti-Mouse Alexa Fluor 647	ThermoFisher Scientific	A31571, RRID:AB_162542	1:500
Goat anti-Rat Alexa Fluor 555	ThermoFisher Scientific	A21434, RRID:AB_141733	1:500 or 1:1000
Goat anti-Rabbit Cy2	Jackson Immuno research	# 111-225-144, RRID:AB_2338021	1:500
Goat anti-Mouse Cy3	Jackson Immuno research	#115-165-166, RRID:AB_2338692	1:500
Goat anti-Mouse Cy5	Jackson Immuno research	#115-175-166, RRID:AB_2338714	1:500
Critical Commercial Assays			
Maxi prep kit	Qiagen	Cat#12362	
RNeasy FFPE RNA isolation kit	Qiagen	Cat# 73504	
NeuroTrace™ 640/660 deep-red fluorescent Nissl stain	Molecular probes	Cat# N-21483, RRID:AB_2572212	
In Situ Cell Death Detection Kit, TMR red (TUNEL)	Sigma-Aldrich	12156792910	
Annexin V Cy5 reagent	Biovision	1013-200	
Click-iT™ EdU Alexa Fluor™ 647 Imaging Kit	Invitrogen	C10340	
Experimental Models: Organisms/Strains			
Ferret *Mustela putorius furo*	Marshall Bioresources	N.A.	
Ferret *Mustela putorius furo*	Euroferret	N.A.	
Oligonucleotides			
Hprt1 FqHprt1_F TACGCTGAGGATTTGGAAAAG	This paper	N.A.	
Hprt1 FqHprt1_R CCATCTCCTTCATCACGTCTC	This paper	N.A.	
ARHGAP11B qARHGAP11B_1F CAGAAAAGAAGGGCGTGTAC	This paper	N.A.	
ARHGAP11B qARHGAP11B_1R GGAGTAGCACAGAGACCATCA	This paper	N.A.	
ARHGAP11B qARHGAP11B_2F TGAGAATAAGATGGATAGCAGCA	This paper	N.A.	
ARHGAP11B qARHGAP11B_2R GGTACACGCCCTTCTTTTCTG	This paper	N.A.	
Recombinant DNA			
pCAGGS	(Florio et al., 2015)	N.A.	
pCAGGS-ARHGAP11B	(Florio et al., 2015)	N.A.	
pCAGGS-mCherry	(Tavano et al., 2018)	N.A.	
pCAGGS-GFP	(Fei et al., 2014)		
Software and Algorithms			
Fiji/ImageJ	Fiji/Imagej	https://imagej.nih.gov/ij/	
Prism	GraphPad software	N.A.	
ZEN	Carl Zeiss	N.A.	

749

750

bioRxiv preprint doi: https://doi.org/10.1101/395830; this version posted August 20, 2018. The copyright holder for this preprint (which was not certified by peer review) is the author/funder. All rights reserved. No reuse allowed without permission.

751 **Experimental animals**

752

753 All experimental procedures were conducted in agreement with the German Animal Welfare
754 Legislation after approval by the Landesdirektion Sachsen (licences TVV 2/2015 and TVV
755 21/2017). Timed-pregnant ferrets (*Mustela putorius furo*) were obtained from Marshall
756 BioResources (NY, USA) or Euroferret (Copenhagen, Denmark) and housed at the Biomedical
757 Services Facility (BMS) of MPI-CBG. Observed mating date was set to E0. Animals were kept in
758 standardized hygienic conditions with free access to food and water and with an 16 h/8 h
759 light/dark cycle. All experiments were performed in the dorsolateral telencephalon of ferret
760 embryos, at a medial position along the rostro-caudal axis, in the prospective motor and
761 somatosensory cortex.

762

763 **Plasmids**

764

765 All plasmids used in this study were previously published (see the Key Resources table). All
766 plasmids were extracted and purified using the EndoFree Plasmid Maxi kit (QIAGEN) following
767 the manufacturer's instructions.

768

769 ***In utero* electroporation of ferrets**

770

771 *In utero* electroporation of ferrets was performed as originally established by Dr. Hiroshi
772 Kawasaki with the modifications listed below (Kawasaki et al., 2012). Pregnant jills (with
773 embryos at E33) were kept fasted for at least 3 h before the surgery. They were first placed in
774 the narcosis box with 4% isoflurane. When in deep anesthesia, the ferrets were placed on the
775 operation table and attached to the narcosis mask with a constant 3% isoflurane flow.
776 Subsequently, the ferrets were injected subcutaneously with analgesic (0.1 ml Metamizol, 50
777 mg/kg), antibiotic (0.13 ml Synulox, 20 mg/kg or 0.1 ml amoxicilin, 10 mg/kg) and glucose (10
778 ml 5% glucose solution). A drop of Dexpanthenol Ointment solution was placed on their eyes
779 to prevent eye dehydration during the surgical procedure. The ferret bellies were then shaved,
780 sterilized with iodide and surgically opened. The uterus was exposed and embryos were
781 injected intraventricularly with a solution containing 0.1% Fast Green (Sigma) in sterile PBS,
782 2.5 µg/µl of either pCAGGS vector (control) or pCAGGS-ARHGAP11B vector, in either case

bioRxiv preprint doi: https://doi.org/10.1101/395830; this version posted August 20, 2018. The copyright holder for this preprint (which was not certified by peer review) is the author/funder. All rights reserved. No reuse allowed without permission.

783 together with 1 µg/µl of pCAGGS vector encoding a fluorescent protein (pCAGGS-GFP or
784 pCAGGS-mCherry). For embryonic studies where the position of the electroporated embryos
785 in the uterus was known, the same fluorescent protein-encoding vector was co-
786 electroporated together with either control or ARHGAP11B-expressing vectors. For postnatal
787 studies, pCAGGS and pCAGGS-ARHGAP11B were co-electroporated with different fluorescent
788 protein-encoding vectors to enable distinction of kits. For different experiments, these vectors
789 were alternated. Electroporations were performed with six 50-msec pulses of 100 V at 1 sec
790 intervals. Following electroporation, uterus was placed back in the peritoneal cavity and the
791 muscle layer with the peritoneum were sutured using a 4-0 suture. The skin was sutured
792 intracutaneously using the same thickness of the suture. Animals were carefully monitored
793 until they woke up and then underwent postoperative care for the following 3 days (2 x daily
794 10 mg/kg amoxicilin, 3 x daily 25 mg/kg Metamizol).
795
796 **EdU labeling of ferret kits**
797
798 For the neurogenic length experiments, a single pulse of EdU was injected intraperitoneally at
799 P5, i.e. 13 days after *in utero* electroporations, and the animals were sacrificed 11 days later,
800 at P16. The protocol for EdU injection was the same as the one previously published for ferret
801 kits (Turrero Garcia et al., 2015).
802
803 **Isolation of ferret brains**
804
805 Ferret embryos were isolated at E37 and E40. Ferret kits were sacrificed at P0, P10 and P16.
806 For the isolation of embryos, pregnant jills underwent the second surgery that followed the
807 same pre-operative care, anesthesia and analgesia as the first surgery. The sutures from the
808 first operation were carefully removed and the uterus was exposed. A caesarian section was
809 made and embryos were removed from the uterus. Subsequently a complete hysterectomy
810 was performed, after which the muscle layer with peritoneum and skin were sutured and the
811 animal underwent the same post-operative care as after the first surgery. Embryonic brains
812 were isolated and fixed at 4°C for 48 h in 4% paraformaldehyde in 120mM phosphate buffer
813 pH 7.4.
814

bioRxiv preprint doi: https://doi.org/10.1101/395830; this version posted August 20, 2018. The copyright holder for this preprint (which was not certified by peer review) is the author/funder. All rights reserved. No reuse allowed without permission.

For the postnatal time points, the kits were sacrificed by intraperitonal injection of 4 mg/kg Xylazin + 40 mg/kg Ketamin. When in deep anaesthesia, the kits were perfused intracardially with PBS, followed by perfusion with 4% paraformaldehyde in 120mM phosphate buffer pH 7.4 at room temperature. Kit brains were then isolated and fixed for 48 h in 4% paraformaldehyde in 120 mM phosphate buffer pH 7.4 at 4°C.

Ferret jills whose kits were used postnatally also underwent the second surgery with the hysterectomy. Upon this surgery, they underwent the same post-operative care as after the first surgery. All jills were kept at the BMS of the MPI-CBG for at least two weeks after the second surgery. Afterwards they were donated for adoption. No adult ferrets were sacrificed in this study.

Preparation of ferret brain slices

Upon fixation ferret brains were sectioned either on a vibratome or cryostat. Vibratome sections were 70 µm thick. Thickness of cryosections varied from 35 to 60 µm. Vibratome sections were either immunostained freshly prepared or conserved in cryoprotectant solution (30% sucrose, 30% ethylene glycol, 1% PVP40, 1.3 mM NaH_2PO_4, 3.9 mM Na_2HPO_4, 15 mM NaCl) and stored at –20°C for later use.

Gene expression analysis by RT-qPCR

For analysis of *ARHGAP11B* expression, total RNA was isolated from two to three cryosections per developmental stage, using the RNeasy FFPE RNA isolation kit (Qiagen) including DNase-treatment following the manufacturer's instructions. An additional DNase-treatment was performed on the isolated RNA using the DNA-free DNA Removal Kit (Life technologies). cDNA was synthesized using random hexamers and Superscript III Reverse Transcriptase (Life Technologies). qPCR was performed using the Light Cycler SYBR green Master mix (Roche) on a Light Cycler 96 (Roche). Gene expression data was normalized based on the housekeeping gene *Hprt1*. Primer sequences are provided in the Key Resources Table.

Immunofluorescence

bioRxiv preprint doi: https://doi.org/10.1101/395830; this version posted August 20, 2018. The copyright holder for this preprint (which was not certified by peer review) is the author/funder. All rights reserved. No reuse allowed without permission.

Immunofluorescence was performed as previously described (Kalebic et al., 2016). Antigen retrieval (1 h incubation with 10 mM citrate buffer pH 6.0 at 70°C in a water bath or oven) was performed for the following samples: all E37 samples, all E40/P0 samples, and vibratome sections of P10 and P16 samples which were used for immunostainings of the nuclear markers (Satb2, Brn2, Sox2, Olig2 and Ki67). When immunofluorescence for Tbr2 (E40/P0) was performed, a modified antigen retrieval protocol was used (1 h incubation with 10 mM citrate buffer pH 6.0 supplemented with 0.05% Tween-20 at 80°C in a water bath). Antigen retrieval was followed by three washes with PBS.

All the immunostainings, except the one for ARHGAP11B, were done as follows. Samples were subjected to permeabilization for 30 min in 0.3% Triton X-100 in PBS at room temperature, followed by quenching for 30 min in 0.1 M glycine in PBS at room temperature. Blocking was performed in a blocking solution (0.2% gelatin, 300 mM NaCl, 0.3% Triton X-100 in PBS) for 30 min. Primary antibodies were incubated in the blocking solution for 48 h at 4°C. Subsequently, the sections were washed three times in the blocking solution, incubated with secondary antibodies (1:500) and DAPI (Sigma) in the blocking solution for 1 h at room temperature, and washed again three times in the blocking solution before being either used for Nissl post-staining or directly mounted on microscopy slides with Mowiol.

For the immunostaining for ARHGAP11B, permeabilization was performed for 1 h in the 0.3% Triton X-100 solution at room temperature. Quenching was performed as for the other immunostainings. Blocking was done in 10% horse serum supplemented with 0.3% Triton X-100 (HS blocking solution) for 1 h. Primary antibodies were incubated in the same solution for 24 h, at 4°C. Subsequently, sections were washed five times in the HS blocking solution, incubated with the secondary antibodies (1:1000) and DAPI in the HS blocking solution for 1 h at room temperature, washed five times in PBS and mounted on microscopy slides with Mowiol. ARHGAP11B antibody used in this study is a mouse monoclonal antibody raised against a recombinant full length ARHGAP11B. As the first 220 amino acids of ARHGAP11B are 89% identical to the first 220 amino acids of the ferret Arhgap11a, we showed by immunostaining that the antibody we used did not recognize the endogenous ferret Arhgap11a (Figure 1 supplement 1E).

bioRxiv preprint doi: https://doi.org/10.1101/395830; this version posted August 20, 2018. The copyright holder for this preprint (which was not certified by peer review) is the author/funder. All rights reserved. No reuse allowed without permission.

Staining with the Nissl fluorescent stain, EdU detection, annexin V labeling, and TUNEL labeling were performed after the antibody stainings. NeuroTrace™ 640/660 deep-red fluorescent Nissl stain (Molecular probes) was used, following the manufacturer's instructions. EdU staining was performed using Click-iT™ EdU Alexa Fluor™ 647 Imaging kit (Invitrogen), following the manufacturer's instructions. Annexin V labeling was performed using the Annexin V-Cy5 bright fluorescence reagent (BioVision), following the manufacturer's instructions. TUNEL labeling was performed using the *In situ* cell death detection kit, TMR red (Sigma-Aldrich), following the manufacturer's instructions.

Image acquisition

Images of whole ferret brains (Figure 4 supplement 3A) were obtained as follows. Images were acquired using an iPhone 7 and taking a photography of the brain through a UV-protection filter mounted on a SZX 16 Olympus stereomicroscope, equipped with a fluorescence lamp.

Fluorescent images were acquired using a Zeiss LSM 880 upright single-photon point scanning confocal system. For the embryonic stages, images were taken as either 1-µm single optical sections with the 40x objective or 2-µm single optical sections with the 20x objective. For the postnatal stages, images were taken as either 2-µm single optical sections with the 20x objective or 7.2 µm single optical sections with the 10x objective. When the images were taken as tile scans, the stitching of the tiles was performed using the ZEN software. Subsequently, all images were analyzed and processed with ImageJ (http://imagej.nih.gov/ij/).

Quantifications

All cell counts were performed in standardized microscopic fields using Fiji, processed using Excel (Microsoft), and results were plotted using Prism (GraphPad Software). For each condition, data (typically at least 3 microscopic fields) from one experiment (see definition below) were pooled, and the mean of the indicated number of experiments was calculated. Whenever possible the quantifications were done blindly.

bioRxiv preprint doi: https://doi.org/10.1101/395830; this version posted August 20, 2018. The copyright holder for this preprint (which was not certified by peer review) is the author/funder. All rights reserved. No reuse allowed without permission.

The definition of the morphological parameters is depicted graphically in the Figure 4 supplement 3D. All the morphological parameters were quantified at two positions in the somatosensory cortex, as defined in Figure 4 supplement 3B, for the following gyri and sulci: posterior sigmoid gyrus, coronal gyrus, lateral gyrus, cruciate sulcus, suprasylvian sulcus and lateral sulcus (Sawada and Watanabe, 2012). All the morphological parameters are presented as a ratio of the value of the electroporated hemisphere and the value of the contralateral hemisphere, as established previously (Matsumoto et al., 2017). Calculations were as follows.

Local Gyrification Index (Local GI): $\frac{The\ length\ of\ the\ inner\ contour}{The\ length\ of\ the\ outer\ contour}$

Local gyrification index is calculated as a ratio of the local GI of the electroporated area and the local GI of the equivalent area on the contralateral side. Gyrus size is calculated as a ratio of the size of an electroporated gyrus ad the size of the equivalent gyrus of the contralateral side. Sulcus depth is calculated as a ratio of the length of the line connecting the outer contour and the bottom of a sulcus and the equivalent line on the contralateral side. Sulcus thickness is calculated as a ratio of the thickness measured from the ventricular surface to the bottom of an electroporated sulcus and the equivalent thickness on the contralateral side. Gyrus thickness is calculated as a ratio of the thickness measured from the ventricular surface to the top of an electroporated gyrus and the equivalent thickness on the contralateral side. The upper layers thickness was measured as distance between the top of layer II and bottom of layer IV. Lateral length of the electroporated area was measured as the distance between the medial-most and the lateral-most cell on a coronal cross-section, following the inner contour of the neocortex. Cell density was measured as amount of DAPI+ nuclei in 50 µm x 50 µm fields.

Statistical analysis

All statistics analyses were conducted using Prism (GraphPad Software). Sample sizes are reported in each figure legend, where the term "one experiment" would refer to one embryo for analysis at E37 or E40, and to one kit for postnatal analysis. Total number of litters analyzed was as follows: E37, 2 litters; E40/P0, 4 litters; P10, 2 litters; P16, 3 litters. Embryos or kits from all litters were included in the statistical analyses. Tests used were Two-way ANOVA with

bioRxiv preprint doi: https://doi.org/10.1101/395830; this version posted August 20, 2018. The copyright holder for this preprint (which was not certified by peer review) is the author/funder. All rights reserved. No reuse allowed without permission.

942 Bonferroni posttest, Student's *t*-test and Mann-Whitney *U*-test. For each quantification, the
943 statistical test and significance are indicated in the figure legend.
944
945

bioRxiv preprint doi: https://doi.org/10.1101/395830; this version posted August 20, 2018. The copyright holder for this preprint (which was not certified by peer review) is the author/funder. All rights reserved. No reuse allowed without permission.

References

Alcamo, E.A., Chirivella, L., Dautzenberg, M., Dobreva, G., Farinas, I., Grosschedl, R., and McConnell, S.K. (2008). Satb2 regulates callosal projection neuron identity in the developing cerebral cortex. Neuron *57*, 364-377.

Arai, Y., Pulvers, J.N., Haffner, C., Schilling, B., Nusslein, I., Calegari, F., and Huttner, W.B. (2011). Neural stem and progenitor cells shorten S-phase on commitment to neuron production. Nat Commun *2*, 154.

Azevedo, F.A.C., Carvalho, L.R.B., Grinberg, L.T., Farfel, J.M., Ferretti, R.E.L., Leite, R.E.P., Jacob, W., Lent, R., and Herculano-Houzel, S. (2009). Equal Numbers of Neuronal and Nonneuronal Cells Make the Human Brain an Isometrically Scaled-Up Primate Brain. J Comp Neurol *513*, 532-541.

Bailey, J.A., Gu, Z., Clark, R.A., Reinert, K., Samonte, R.V., Schwartz, S., Adams, M.D., Myers, E.W., Li, P.W., and Eichler, E.E. (2002). Recent segmental duplications in the human genome. Science *297*, 1003-1007.

Barnette, A.R., Neil, J.J., Kroenke, C.D., Griffith, J.L., Epstein, A.A., Bayly, P.V., Knutsen, A.K., and Inder, T.E. (2009). Characterization of brain development in the ferret via MRI. Pediatr Res *66*, 80-84.

Betizeau, M., Cortay, V., Patti, D., Pfister, S., Gautier, E., Bellemin-Ménard, A., Afanassieff, M., Huissoud, C., Douglas, R.J., Kennedy, H.*, et al.* (2013). Precursor diversity and complexity of lineage relationships in the outer subventricular zone of the primate. Neuron *80*, 442-457.

Borrell, V. (2018). How Cells Fold the Cerebral Cortex. J Neurosci *38*, 776-783.

Borrell, V., and Götz, M. (2014). Role of radial glial cells in cerebral cortex folding. Curr Opin Neurobiol *27*, 39-46.

Borrell, V., and Reillo, I. (2012). Emerging roles of neural stem cells in cerebral cortex development and evolution. Dev Neurobiol *72*, 955-971.

Britanova, O., de Juan Romero, C., Cheung, A., Kwan, K.Y., Schwark, M., Gyorgy, A., Vogel, T., Akopov, S., Mitkovski, M., Agoston, D.*, et al.* (2008). Satb2 is a postmitotic determinant for upper-layer neuron specification in the neocortex. Neuron *57*, 378-392.

Dehay, C., Kennedy, H., and Kosik, K.S. (2015). The outer subventricular zone and primate-specific cortical complexification. Neuron *85*, 683-694.

bioRxiv preprint doi: https://doi.org/10.1101/395830; this version posted August 20, 2018. The copyright holder for this preprint (which was not certified by peer review) is the author/funder. All rights reserved. No reuse allowed without permission.

976 Dennis, M.Y., and Eichler, E.E. (2016). Human adaptation and evolution by segmental
977 duplication. Curr Opin Genet Dev *41*, 44-52.

978 Dennis, M.Y., Harshman, L., Nelson, B.J., Penn, O., Cantsilieris, S., Huddleston, J., Antonacci,
979 F., Penewit, K., Denman, L., Raja, A.*, et al.* (2017). The evolution and population diversity of
980 human-specific segmental duplications. Nat Ecol Evol *1*, 69.

981 Dominguez, M.H., Ayoub, A.E., and Rakic, P. (2013). POU-III transcription factors (Brn1, Brn2,
982 and Oct6) influence neurogenesis, molecular identity, and migratory destination of upper-
983 layer cells of the cerebral cortex. Cereb Cortex *23*, 2632-2643.

984 Englund, C., Fink, A., Lau, C., Pham, D., Daza, R.A., Bulfone, A., Kowalczyk, T., and Hevner,
985 R.F. (2005). Pax6, Tbr2, and Tbr1 are expressed sequentially by radial glia, intermediate
986 progenitor cells, and postmitotic neurons in developing neocortex. J Neurosci *25*, 247-251.

987 Fame, R.M., MacDonald, J.L., and Macklis, J.D. (2011). Development, specification, and
988 diversity of callosal projection neurons. Trends Neurosci *34*, 41-50.

989 Fei, J.F., Haffner, C., and Huttner, W.B. (2014). 3' UTR-dependent, miR-92-mediated
990 restriction of Tis21 expression maintains asymmetric neural stem cell division to ensure
991 proper neocortex size. Cell Rep *7*, 398-411.

992 Fernandez, V., Llinares-Benadero, C., and Borrell, V. (2016). Cerebral cortex expansion and
993 folding: what have we learned? The EMBO journal *35*, 1021-1044.

994 Fiddes, I.T., Lodewijk, G.A., Mooring, M., Bosworth, C.M., Ewing, A.D., Mantalas, G.L., Novak,
995 A.M., van den Bout, A., Bishara, A., Rosenkrantz, J.L.*, et al.* (2018). Human-Specific
996 NOTCH2NL Genes Affect Notch Signaling and Cortical Neurogenesis. Cell *173*, 1356-1369
997 e1322.

998 Fietz, S.A., Kelava, I., Vogt, J., Wilsch-Brauninger, M., Stenzel, D., Fish, J.L., Corbeil, D., Riehn,
999 A., Distler, W., Nitsch, R.*, et al.* (2010). OSVZ progenitors of human and ferret neocortex are
1000 epithelial-like and expand by integrin signaling. Nat Neurosci *13*, 690-699.

1001 Florio, M., Albert, M., Taverna, E., Namba, T., Brandl, H., Lewitus, E., Haffner, C., Sykes, A.,
1002 Wong, F.K., Peters, J.*, et al.* (2015). Human-specific gene ARHGAP11B promotes basal
1003 progenitor amplification and neocortex expansion. Science *347*, 1465-1470.

1004 Florio, M., Heide, M., Pinson, A., Brandl, H., Albert, M., Winkler, S., Wimberger, P., Huttner,
1005 W.B., and Hiller, M. (2018). Evolution and cell-type specificity of human-specific genes
1006 preferentially expressed in progenitors of fetal neocortex. Elife *7*, e32332.

bioRxiv preprint doi: https://doi.org/10.1101/395830; this version posted August 20, 2018. The copyright holder for this preprint (which was not certified by peer review) is the author/funder. All rights reserved. No reuse allowed without permission.

1007 Florio, M., and Huttner, W.B. (2014). Neural progenitors, neurogenesis and the evolution of
1008 the neocortex. Development *141*, 2182-2194.

1009 Florio, M., Namba, T., Pääbo, S., Hiller, M., and Huttner, W.B. (2016). A single splice site
1010 mutation in human-specific ARHGAP11B causes basal progenitor amplification.
1011 Science Advances *2*.

1012 Gertz, C.C., and Kriegstein, A.R. (2015). Neuronal Migration Dynamics in the Developing
1013 Ferret Cortex. J Neurosci *35*, 14307-14315.

1014 Geschwind, D.H., and Rakic, P. (2013). Cortical evolution: judge the brain by its cover.
1015 Neuron *80*, 633-647.

1016 Götz, M., and Huttner, W.B. (2005). The cell biology of neurogenesis. Nat Rev Mol Cell Biol *6*,
1017 777-788.

1018 Hansen, D.V., Lui, J.H., Parker, P.R., and Kriegstein, A.R. (2010). Neurogenic radial glia in the
1019 outer subventricular zone of human neocortex. Nature *464*, 554-561.

1020 Herculano-Houzel, S., Catania, K., Manger, P.R., and Kaas, J.H. (2015). Mammalian Brains Are
1021 Made of These: A Dataset of the Numbers and Densities of Neuronal and Nonneuronal Cells
1022 in the Brain of Glires, Primates, Scandentia, Eulipotyphlans, Afrotherians and Artiodactyls,
1023 and Their Relationship with Body Mass. Brain Behav Evol *86*, 145-163.

1024 Hutsler, J.J., Lee, D.G., and Porter, K.K. (2005). Comparative analysis of cortical layering and
1025 supragranular layer enlargement in rodent carnivore and primate species. Brain Res *1052*,
1026 71-81.

1027 Jackson, C.A., Peduzzi, J.D., and Hickey, T.L. (1989). Visual cortex development in the ferret.
1028 I. Genesis and migration of visual cortical neurons. J Neurosci *9*, 1242-1253.

1029 Jardim-Messeder, D., Lambert, K., Noctor, S., Pestana, F.M., de Castro Leal, M.E., Bertelsen,
1030 M.F., Alagaili, A.N., Mohammad, O.B., Manger, P.R., and Herculano-Houzel, S. (2017). Dogs
1031 Have the Most Neurons, Though Not the Largest Brain: Trade-Off between Body Mass and
1032 Number of Neurons in the Cerebral Cortex of Large Carnivoran Species. Front Neuroanat *11*,
1033 118.

1034 Kaas, J.H. (2013). The evolution of brains from early mammals to humans. Wiley Interdiscip
1035 Rev Cogn Sci *4*, 33-45.

bioRxiv preprint doi: https://doi.org/10.1101/395830; this version posted August 20, 2018. The copyright holder for this preprint (which was not certified by peer review) is the author/funder. All rights reserved. No reuse allowed without permission.

1036 Kagawa, Y., Matsumoto, S., Kamioka, Y., Mimori, K., Naito, Y., Ishii, T., Okuzaki, D., Nishida,
1037 N., Maeda, S., Naito, A.*, et al.* (2013). Cell cycle-dependent Rho GTPase activity dynamically
1038 regulates cancer cell motility and invasion in vivo. PloS One *8*, e83629.

1039 Kalebic, N., Long, K., and Huttner, W.B. (2017). Neocortex Expansion in Development and
1040 Evolution: The Cell Biology of Neural Stem and Progenitor Cells and the Impact of Human-
1041 Specific Gene Expression. In Evolution of Nervous Systems 2e, J. Kaas, ed. (Oxford: Elsevier),
1042 pp. 73-89.

1043 Kalebic, N., Taverna, E., Tavano, S., Wong, F.K., Suchold, D., Winkler, S., Huttner, W.B., and
1044 Sarov, M. (2016). CRISPR/Cas9-induced disruption of gene expression in mouse embryonic
1045 brain and single neural stem cells in vivo. EMBO Rep *17*, 338-348.

1046 Kawasaki, H. (2014). Molecular investigations of the brain of higher mammals using
1047 gyrencephalic carnivore ferrets. Neurosci Res *86*, 59-65.

1048 Kawasaki, H., Iwai, L., and Tanno, K. (2012). Rapid and efficient genetic manipulation of
1049 gyrencephalic carnivores using in utero electroporation. Mol Brain *5*, 24.

1050 Kawasaki, H., Toda, T., and Tanno, K. (2013). In vivo genetic manipulation of cortical
1051 progenitors in gyrencephalic carnivores using in utero electroporation. Biology Open *2*, 95-
1052 100.

1053 Kolk, S.M., Whitman, M.C., Yun, M.E., Shete, P., and Donoghue, M.J. (2006). A unique
1054 subpopulation of Tbr1-expressing deep layer neurons in the developing cerebral cortex. Mol
1055 Cell Neurosci *32*, 200-214.

1056 Kroenke, C.D., and Bayly, P.V. (2018). How Forces Fold the Cerebral Cortex. J Neurosci *38*,
1057 767-775.

1058 Krubitzer, L. (2007). The magnificent compromise: cortical field evolution in mammals.
1059 Neuron *56*, 201-208.

1060 LaMonica, B.E., Lui, J.H., Hansen, D.V., and Kriegstein, A.R. (2013). Mitotic spindle
1061 orientation predicts outer radial glial cell generation in human neocortex. Nat Commun *4*,
1062 1665.

1063 Lewitus, E., Hof, P.R., and Sherwood, C.C. (2012). Phylogenetic comparison of neuron and
1064 glia densities in the primary visual cortex and hippocampus of carnivores and primates.
1065 Evolution *66*, 2551-2563.

bioRxiv preprint doi: https://doi.org/10.1101/395830; this version posted August 20, 2018. The copyright holder for this preprint (which was not certified by peer review) is the author/funder. All rights reserved. No reuse allowed without permission.

1066 Lewitus, E., Kelava, I., Kalinka, A.T., Tomancak, P., and Huttner, W.B. (2014). An adaptive
1067 threshold in mammalian neocortical evolution. PLoS Biol *12*, e1002000.

1068 Lodato, S., and Arlotta, P. (2015). Generating neuronal diversity in the mammalian cerebral
1069 cortex. Annu Rev Cell Dev Biol *31*, 699-720.

1070 Lopez-Hidalgo, M., Hoover, W.B., and Schummers, J. (2016). Spatial organization of
1071 astrocytes in ferret visual cortex. J Comp Neurol *524*, 3561-3576.

1072 Lui, J.H., Hansen, D.V., and Kriegstein, A.R. (2011). Development and evolution of the human
1073 neocortex. Cell *146*, 18-36.

1074 Martinez-Martinez, M.A., De Juan Romero, C., Fernandez, V., Cardenas, A., Götz, M., and
1075 Borrell, V. (2016). A restricted period for formation of outer subventricular zone defined by
1076 Cdh1 and Trnp1 levels. Nat Commun *7*, 11812.

1077 Matsumoto, N., Shinmyo, Y., Ichikawa, Y., and Kawasaki, H. (2017). Gyrification of the
1078 cerebral cortex requires FGF signaling in the mammalian brain. Elife *6*.

1079 McEvilly, R.J., de Diaz, M.O., Schonemann, M.D., Hooshmand, F., and Rosenfeld, M.G.
1080 (2002). Transcriptional regulation of cortical neuron migration by POU domain factors.
1081 Science *295*, 1528-1532.

1082 Mo, Z., and Zecevic, N. (2009). Human fetal radial glia cells generate oligodendrocytes in
1083 vitro. Glia *57*, 490-498.

1084 Molnar, Z., Metin, C., Stoykova, A., Tarabykin, V., Price, D.J., Francis, F., Meyer, G., Dehay, C.,
1085 and Kennedy, H. (2006). Comparative aspects of cerebral cortical development. Eur J
1086 Neurosci *23*, 921-934.

1087 Molyneaux, B.J., Arlotta, P., Menezes, J.R., and Macklis, J.D. (2007). Neuronal subtype
1088 specification in the cerebral cortex. Nat Rev Neurosci *8*, 427-437.

1089 Otani, T., Marchetto, M.C., Gage, F.H., Simons, B.D., and Livesey, F.J. (2016). 2D and 3D Stem
1090 Cell Models of Primate Cortical Development Identify Species-Specific Differences in
1091 Progenitor Behavior Contributing to Brain Size. Cell Stem Cell *18*, 467-480.

1092 Pollen, A.A., Nowakowski, T.J., Chen, J., Retallack, H., Sandoval-Espinosa, C., Nicholas, C.R.,
1093 Shuga, J., Liu, S.J., Oldham, M.C., Diaz, A.*, et al.* (2015). Molecular Identity of Human Outer
1094 Radial Glia during Cortical Development. Cell *163*, 55-67.

bioRxiv preprint doi: https://doi.org/10.1101/395830; this version posted August 20, 2018. The copyright holder for this preprint (which was not certified by peer review) is the author/funder. All rights reserved. No reuse allowed without permission.

1095 Poluch, S., and Juliano, S.L. (2015). Fine-tuning of neurogenesis is essential for the
1096 evolutionary expansion of the cerebral cortex. Cereb Cortex *25*, 346-364.

1097 Rakic, P. (1972). Mode of cell migration to the superficial layers of fetal monkey neocortex. J
1098 Comp Neurol *145*, 61-83.

1099 Rakic, P. (1978). Neuronal migration and contact guidance in the primate telencephalon.
1100 Postgraduate Medical Journal *54 Suppl 1*, 25-40.

1101 Rakic, P. (2003a). Developmental and evolutionary adaptations of cortical radial glia. Cereb
1102 Cortex *13*, 541-549.

1103 Rakic, P. (2003b). Elusive radial glial cells: historical and evolutionary perspective. Glia *43*,
1104 19-32.

1105 Rakic, P. (2009). Evolution of the neocortex: a perspective from developmental biology. Nat
1106 Rev Neurosci *10*, 724-735.

1107 Reillo, I., de Juan Romero, C., Garcia-Cabezas, M.A., and Borrell, V. (2011). A role for
1108 intermediate radial glia in the tangential expansion of the mammalian cerebral cortex. Cereb
1109 Cortex *21*, 1674-1694.

1110 Sawada, K., and Watanabe, M. (2012). Development of cerebral sulci and gyri in ferrets
1111 (Mustela putorius). Congenital anomalies *52*, 168-175.

1112 Shinmyo, Y., Terashita, Y., Dinh Duong, T.A., Horiike, T., Kawasumi, M., Hosomichi, K., Tajima,
1113 A., and Kawasaki, H. (2017). Folding of the Cerebral Cortex Requires Cdk5 in Upper-Layer
1114 Neurons in Gyrencephalic Mammals. Cell Rep *20*, 2131-2143.

1115 Shitamukai, A., Konno, D., and Matsuzaki, F. (2011). Oblique radial glial divisions in the
1116 developing mouse neocortex induce self-renewing progenitors outside the germinal zone
1117 that resemble primate outer subventricular zone progenitors. J Neurosci *31*, 3683-3695.

1118 Sidman, R.L., and Rakic, P. (1973). Neuronal migration, with special reference to developing
1119 human brain: a review. Brain research *62*, 1-35.

1120 Smart, I.H., Dehay, C., Giroud, P., Berland, M., and Kennedy, H. (2002). Unique morphological
1121 features of the proliferative zones and postmitotic compartments of the neural epithelium
1122 giving rise to striate and extrastriate cortex in the monkey. Cerebal Cortex *12*, 37-53.

bioRxiv preprint doi: https://doi.org/10.1101/395830; this version posted August 20, 2018. The copyright holder for this preprint (which was not certified by peer review) is the author/funder. All rights reserved. No reuse allowed without permission.

1123 Smart, I.H., and McSherry, G.M. (1986a). Gyrus formation in the cerebral cortex in the ferret.
1124 I. Description of the external changes. J Anat *146*, 141-152.

1125 Smart, I.H., and McSherry, G.M. (1986b). Gyrus formation in the cerebral cortex of the
1126 ferret. II. Description of the internal histological changes. J Anat *147*, 27-43.

1127 Sousa, A.M.M., Meyer, K.A., Santpere, G., Gulden, F.O., and Sestan, N. (2017). Evolution of
1128 the Human Nervous System Function, Structure, and Development. Cell *170*, 226-247.

1129 Sugitani, Y., Nakai, S., Minowa, O., Nishi, M., Jishage, K., Kawano, H., Mori, K., Ogawa, M.,
1130 and Noda, T. (2002). Brn-1 and Brn-2 share crucial roles in the production and positioning of
1131 mouse neocortical neurons. Genes Dev *16*, 1760-1765.

1132 Suzuki, I.K., Gacquer, D., Van Heurck, R., Kumar, D., Wojno, M., Bilheu, A., Herpoel, A.,
1133 Lambert, N., Cheron, J., Polleux, F*., et al.* (2018). Human-Specific NOTCH2NL Genes Expand
1134 Cortical Neurogenesis through Delta/Notch Regulation. Cell *173*, 1370-1384 e1316.

1135 Tarabykin, V., Stoykova, A., Usman, N., and Gruss, P. (2001). Cortical upper layer neurons
1136 derive from the subventricular zone as indicated by Svet1 gene expression. Development
1137 *128*, 1983-1993.

1138 Tavano, S., Taverna, E., Kalebic, N., Haffner, C., Namba, T., Dahl, A., Wilsch-Brauninger, M.,
1139 Paridaen, J., and Huttner, W.B. (2018). Insm1 Induces Neural Progenitor Delamination in
1140 Developing Neocortex via Downregulation of the Adherens Junction Belt-Specific Protein
1141 Plekha7. Neuron *97*, 1299-1314 e1298.

1142 Turrero Garcia, M., Chang, Y., Arai, Y., and Huttner, W.B. (2015). S-phase duration is the
1143 main target of cell cycle regulation in neural progenitors of developing ferret neocortex. J
1144 Comp Neurol *524*, 456-470.

1145 Voigt, T. (1989). Development of glial cells in the cerebral wall of ferrets: direct tracing of
1146 their transformation from radial glia into astrocytes. J Comp Neurol *289*, 74-88.

1147 Wang, X., Tsai, J.W., LaMonica, B., and Kriegstein, A.R. (2011). A new subtype of progenitor
1148 cell in the mouse embryonic neocortex. Nature Neuroscience *14*, 555-561.

1149 Wilsch-Bräuninger, M., Florio, M., and Huttner, W.B. (2016). Neocortex expansion in
1150 development and evolution - from cell biology to single genes. Current opinion in
1151 neurobiology *39*, 122-132.

bioRxiv preprint doi: https://doi.org/10.1101/395830; this version posted August 20, 2018. The copyright holder for this preprint (which was not certified by peer review) is the author/funder. All rights reserved. No reuse allowed without permission.

1152 Wong, F.K., Fei, J.F., Mora-Bermudez, F., Taverna, E., Haffner, C., Fu, J., Anastassiadis, K.,
1153 Stewart, A.F., and Huttner, W.B. (2015). Sustained Pax6 Expression Generates Primate-like
1154 Basal Radial Glia in Developing Mouse Neocortex. PLoS Biology *13*, e1002217.
1155

bioRxiv preprint doi: https://doi.org/10.1101/395830; this version posted August 20, 2018. The copyright holder for this preprint (which was not certified by peer review) is the author/funder. All rights reserved. No reuse allowed without permission.

Figure 1

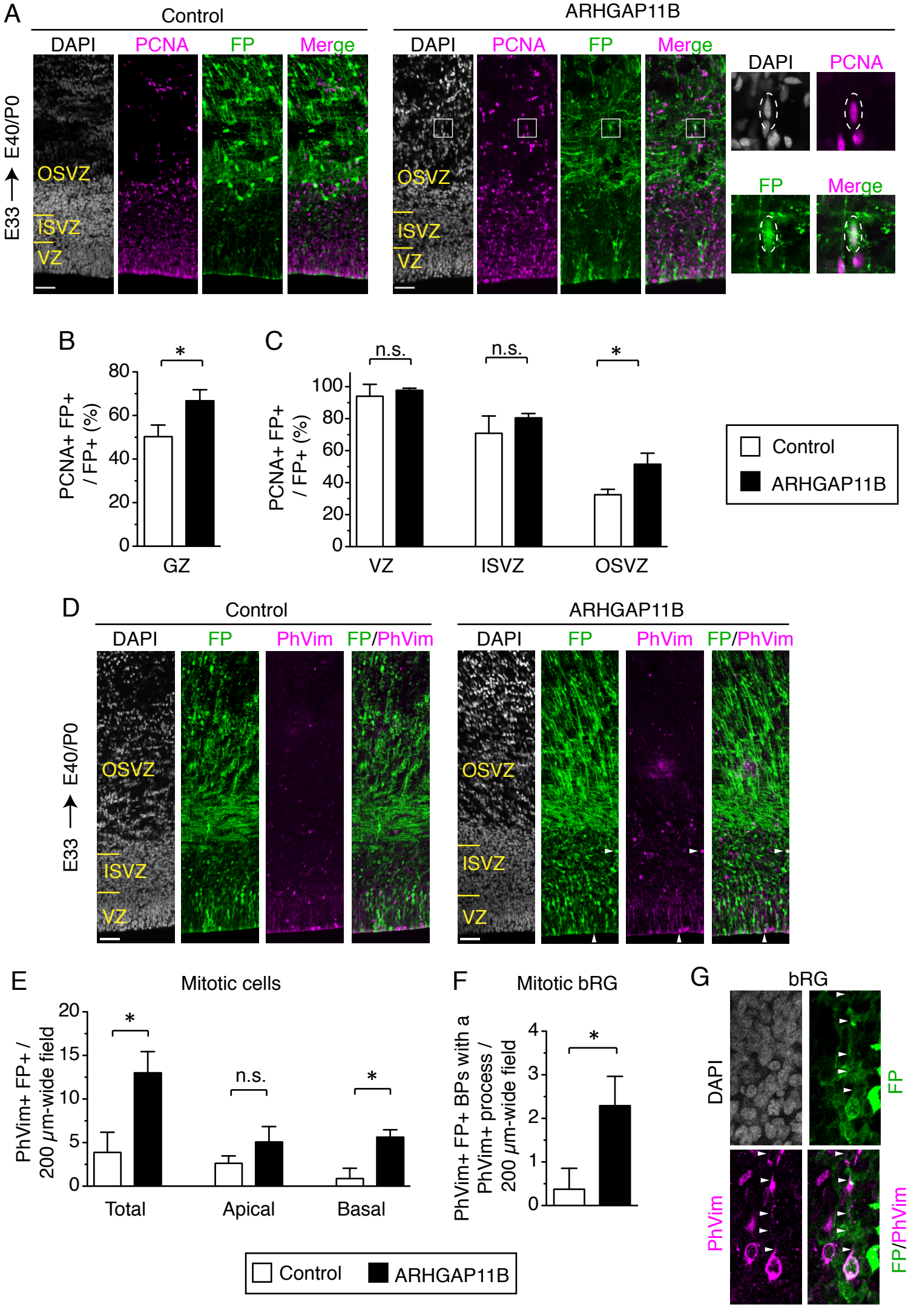

Figure 2

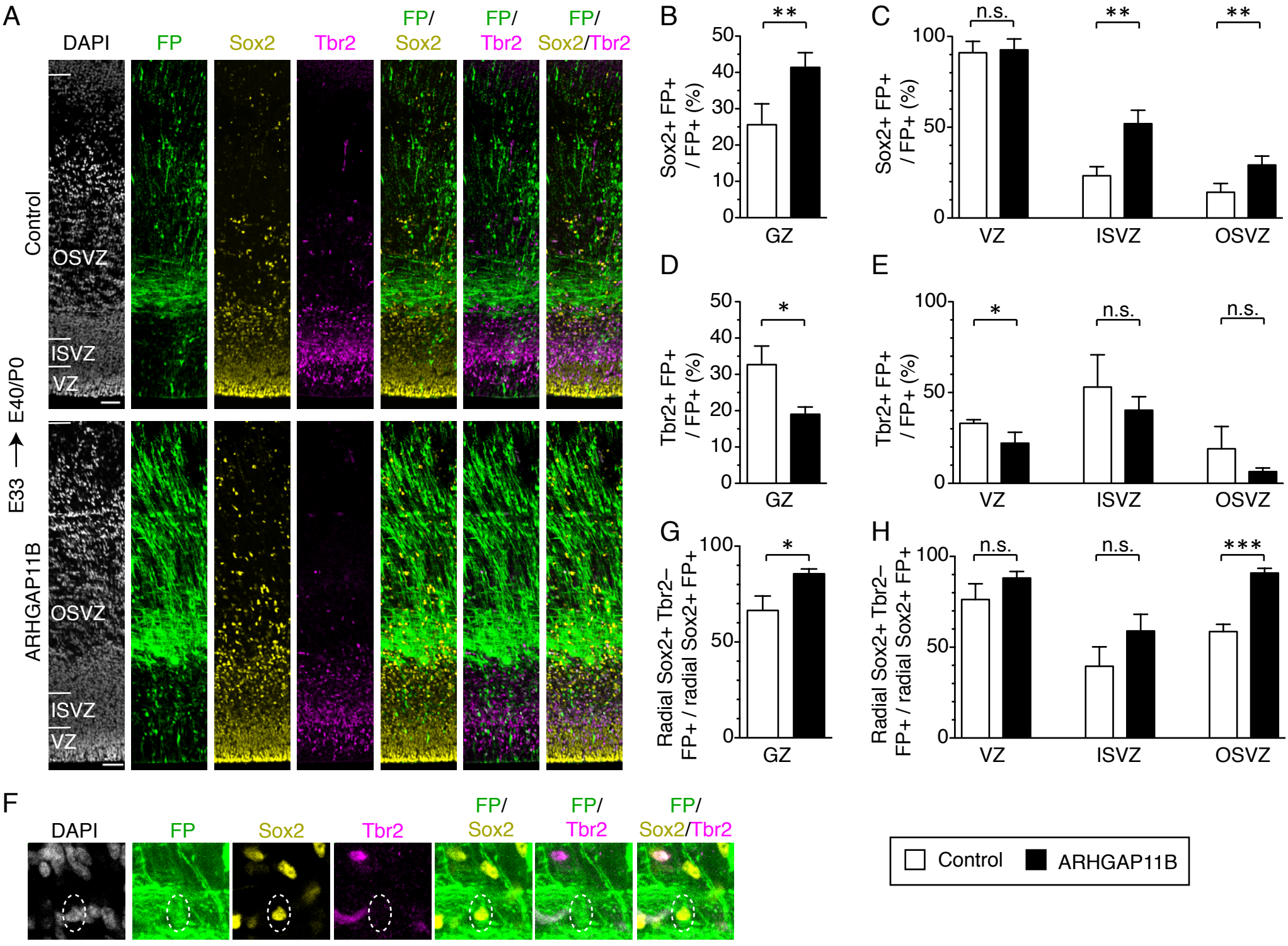
A
DAPI
FP
Sox2
Tbr2
FP/ Sox2
FP/ Tbr2
FP/ Sox2/Tbr2
Control
OSVZ
ISVZ
VZ
E33 → E40/P0
ARHGAP11B
OSVZ
ISVZ
VZ
B
Sox2+ FP+ / FP+ (%)
GZ
C
Sox2+ FP+ / FP+ (%)
VZ
ISVZ
OSVZ
n.s.
D
Tbr2+ FP+ / FP+ (%)
GZ
E
Tbr2+ FP+ / FP+ (%)
VZ
ISVZ
OSVZ
n.s.
G
Radial Sox2+ Tbr2– FP+ / radial Sox2+ FP+
GZ
H
Radial Sox2+ Tbr2– FP+ / radial Sox2+ FP+
VZ
ISVZ
OSVZ
n.s.
F
DAPI
FP
Sox2
Tbr2
FP/ Sox2
FP/ Tbr2
FP/ Sox2/Tbr2
Control
ARHGAP11B

Figure 3

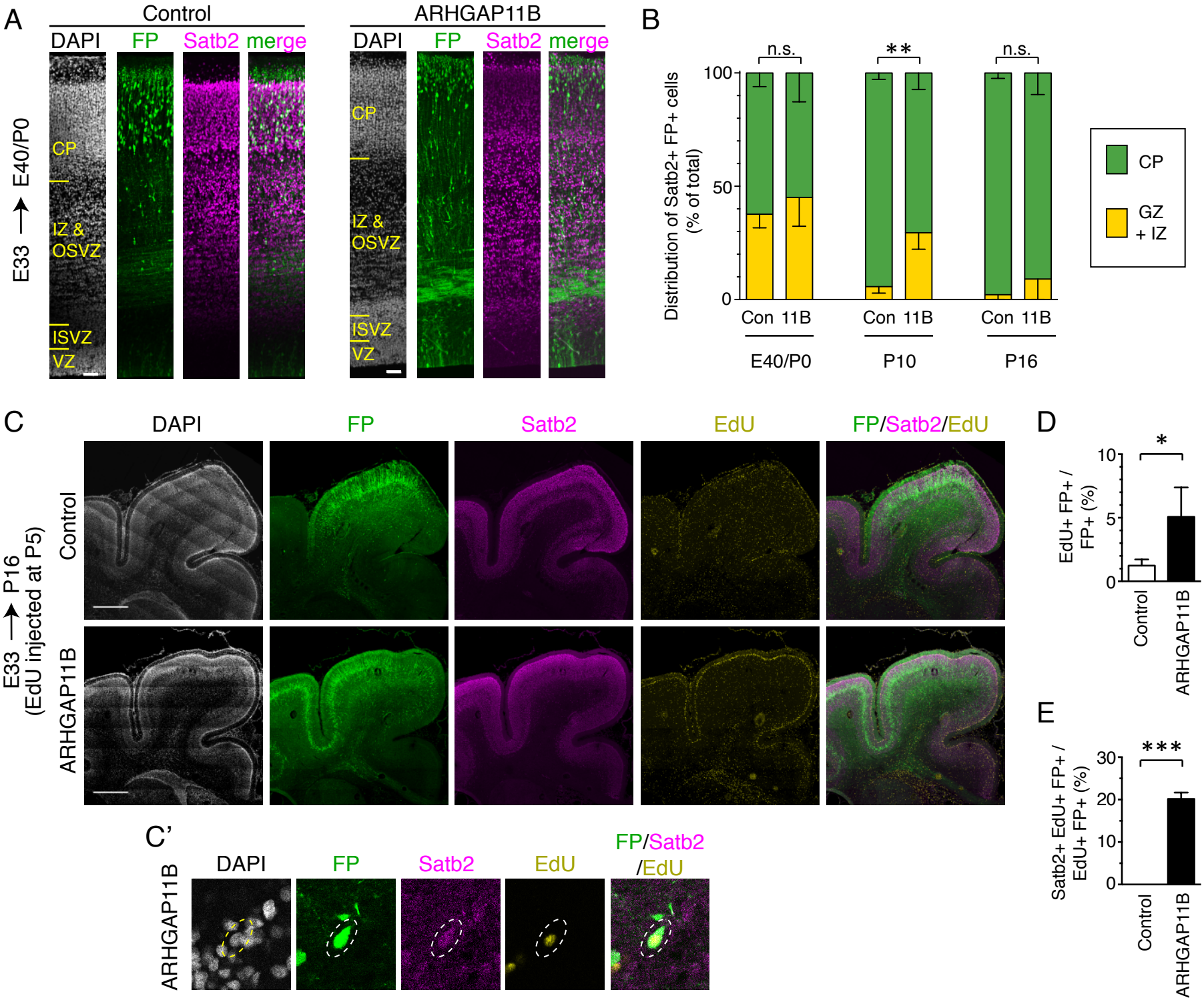
A
Control
ARHGAP11B
DAPI
FP
Satb2
merge
E33 → E40/P0
CP
IZ &
OSVZ
ISVZ
VZ
B
Distribution of Satb2+ FP+ cells (% of total)
100
50
0
n.s.
**
n.s.
Con
11B
E40/P0
P10
P16
CP
GZ
+ IZ
C
DAPI
FP
Satb2
EdU
FP/Satb2/EdU
E33 → P16
(EdU injected at P5)
Control
ARHGAP11B
C'
FP/Satb2
/EdU
D
EdU+ FP+ /
FP+ (%)
*
10
5
0
Control
ARHGAP11B
E
Satb2+ EdU+ FP+ /
EdU+ FP+ (%)
***
30
20
10
0

Figure 4

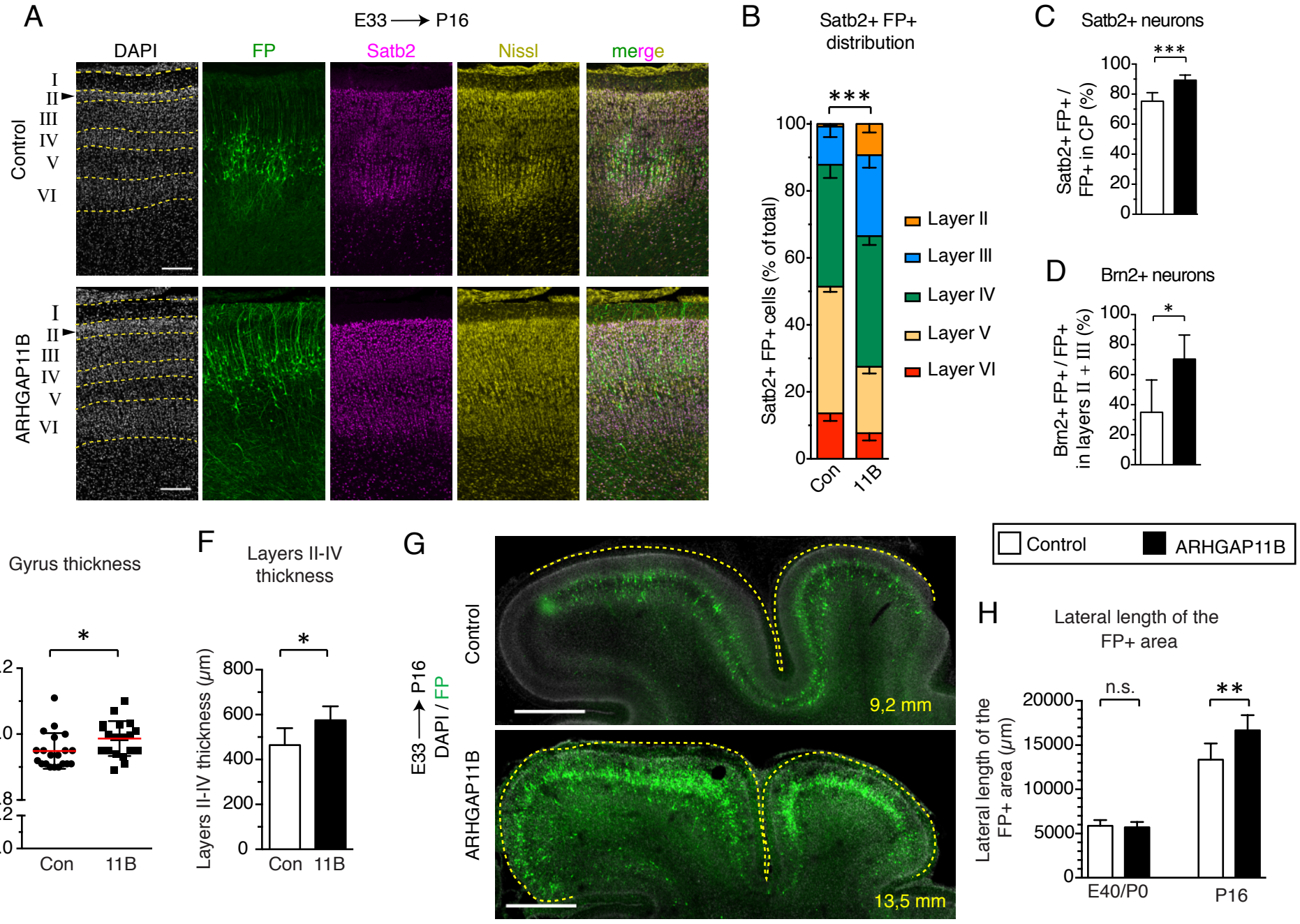
A
E33 → P16
DAPI
FP
Satb2
Nissl
merge
Control
ARHGAP11B
I
II
III
IV
V
VI
B
Satb2+ FP+ distribution
***
Satb2+ FP+ cells (% of total)
100
80
60
40
20
0
Con
11B
Layer II
Layer III
Layer IV
Layer V
Layer VI
C
Satb2+ neurons
***
Satb2+ FP+ / FP+ in CP (%)
D
Brn2+ neurons
*
Brn2+ FP+ / FP+ in layers II + III (%)
E
Gyrus thickness
*
Gyrus thickness IUE/ gyrus thickness non-IUE
1.2
1.0
0.8
0.2
0.0
Con
11B
F
Layers II-IV thickness
*
Layers II-IV thickness (μm)
800
600
400
200
0
Con
11B
G
E33 → P16
DAPI / FP
Control
ARHGAP11B
9,2 mm
13,5 mm
Control
ARHGAP11B
H
Lateral length of the FP+ area
n.s.
**
Lateral length of the FP+ area (μm)
20000
15000
10000
5000
0
E40/P0
P16

bioRxiv preprint doi: https://doi.org/10.1101/395830; this version posted August 20, 2018. The copyright holder for this preprint (which was not certified by peer review) is the author/funder. All rights reserved. No reuse allowed without permission.

Figure 1-supplement 1

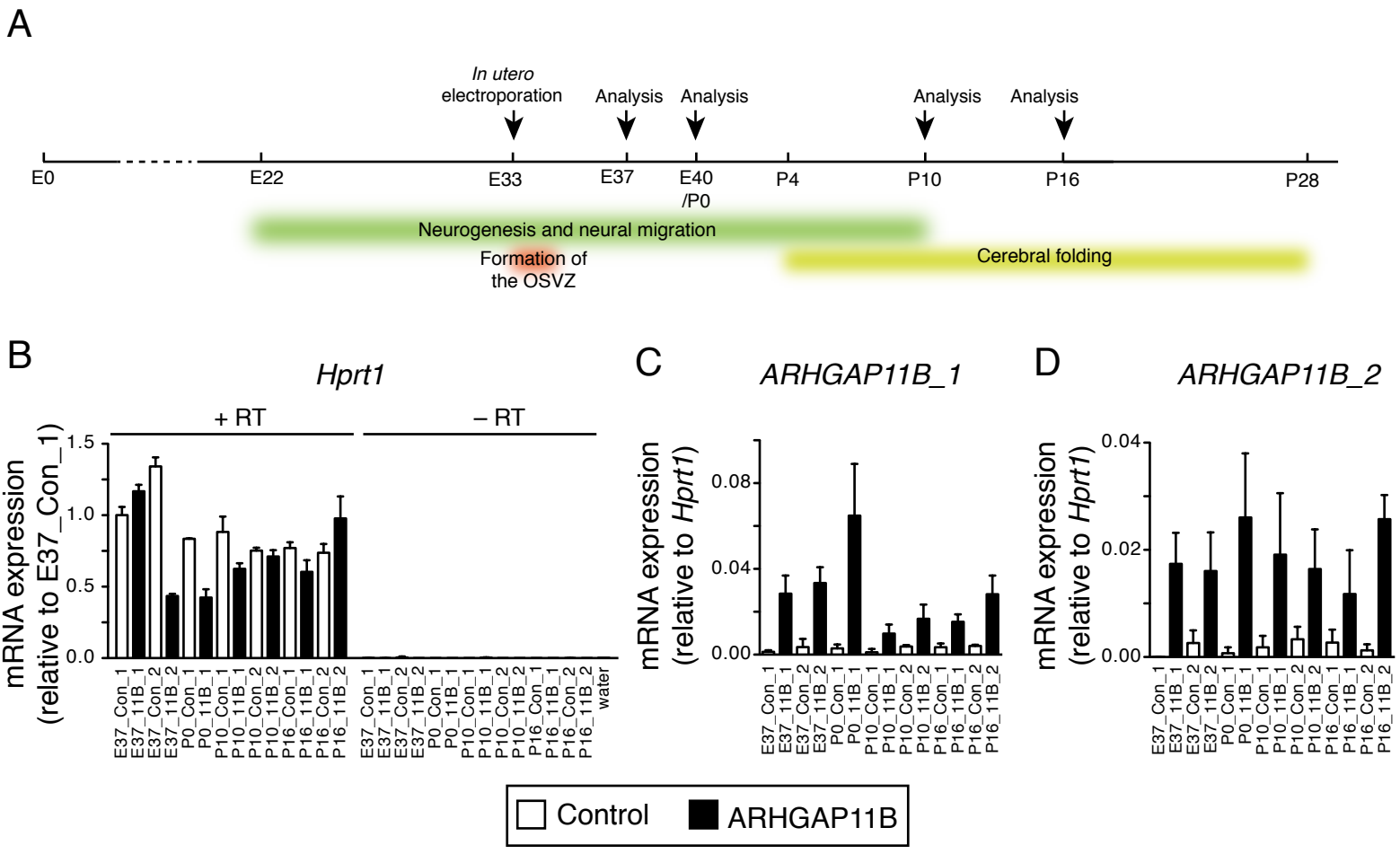

bioRxiv preprint doi: https://doi.org/10.1101/395830; this version posted August 20, 2018. The copyright holder for this preprint (which was not certified by peer review) is the author/funder. All rights reserved. No reuse allowed without permission.

Figure 3 supplement 1

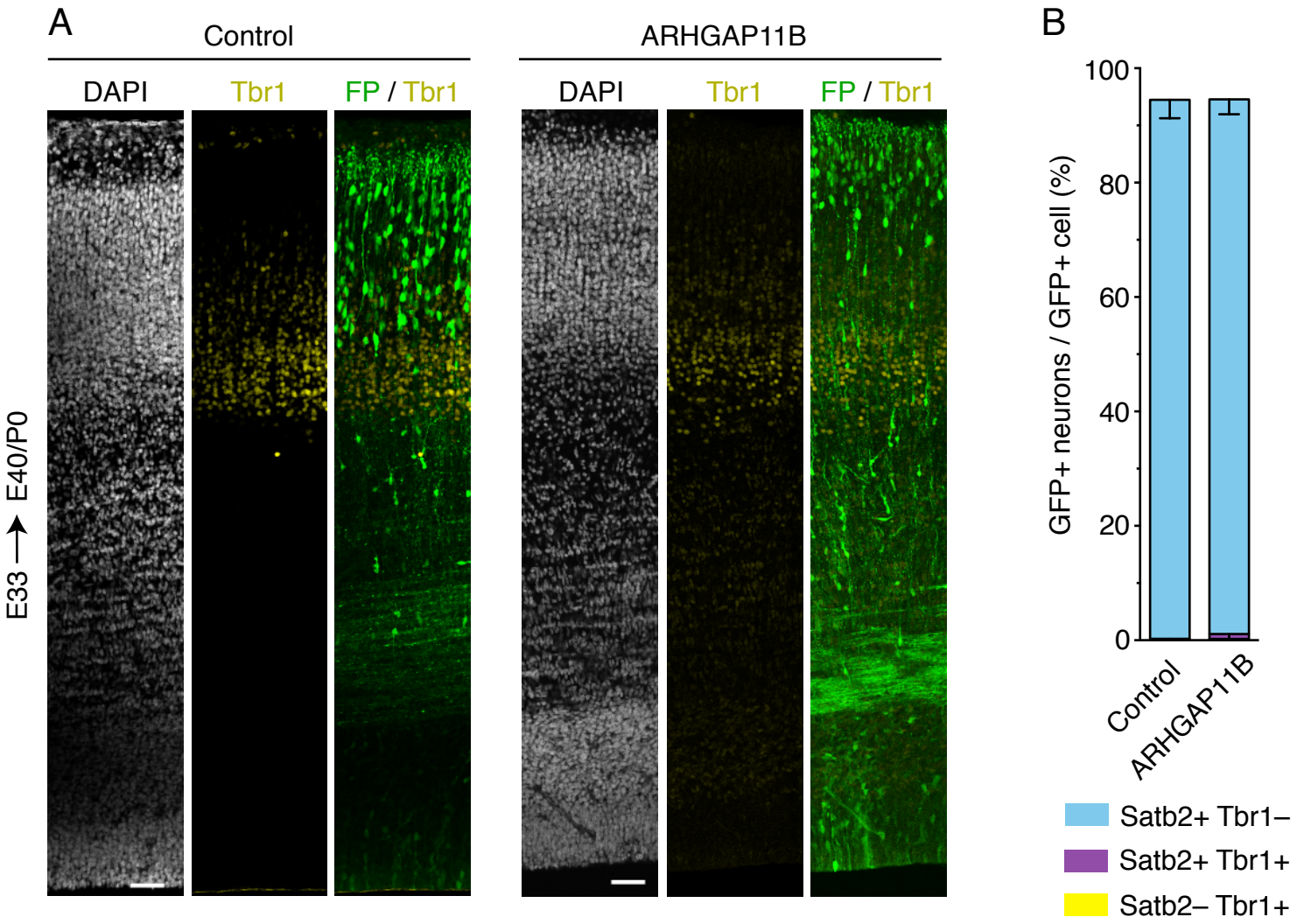

Figure 3 supplement 2

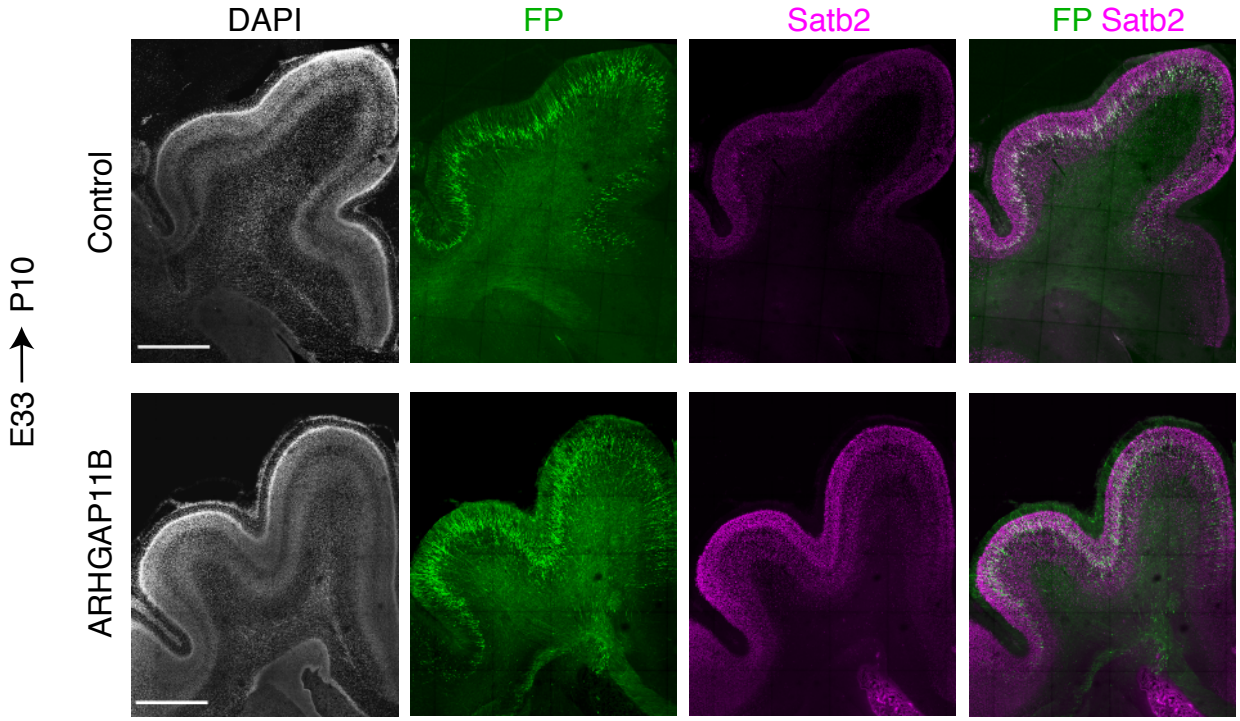

bioRxiv preprint doi: https://doi.org/10.1101/395830; this version posted August 20, 2018. The copyright holder for this preprint (which was not certified by peer review) is the author/funder. All rights reserved. No reuse allowed without permission.

Figure 4 supplement 1

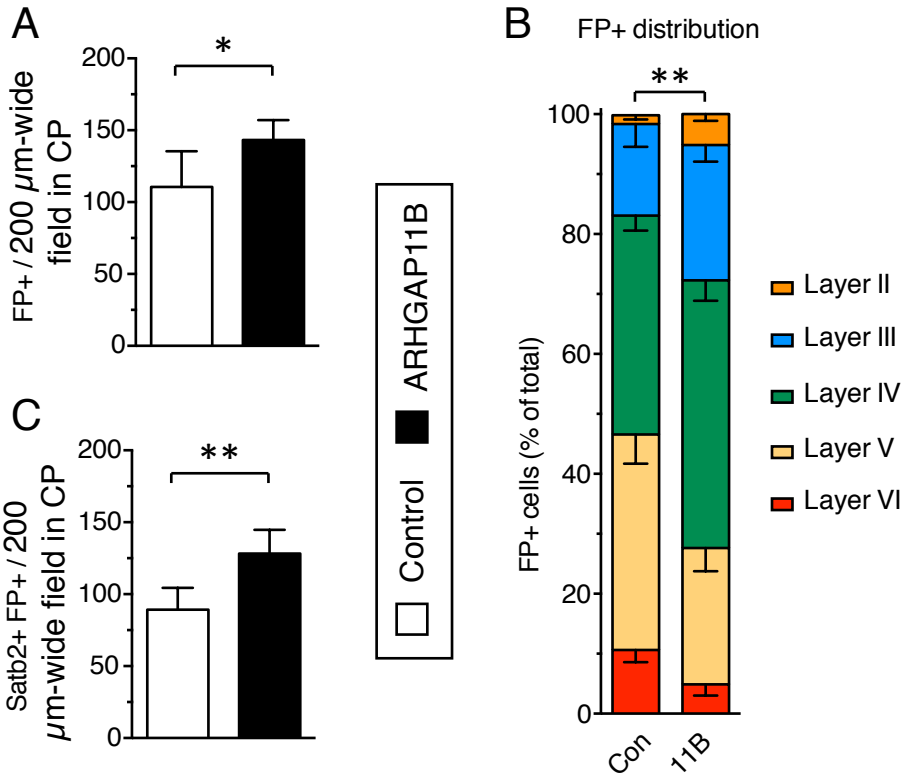

Figure 4 supplement 2

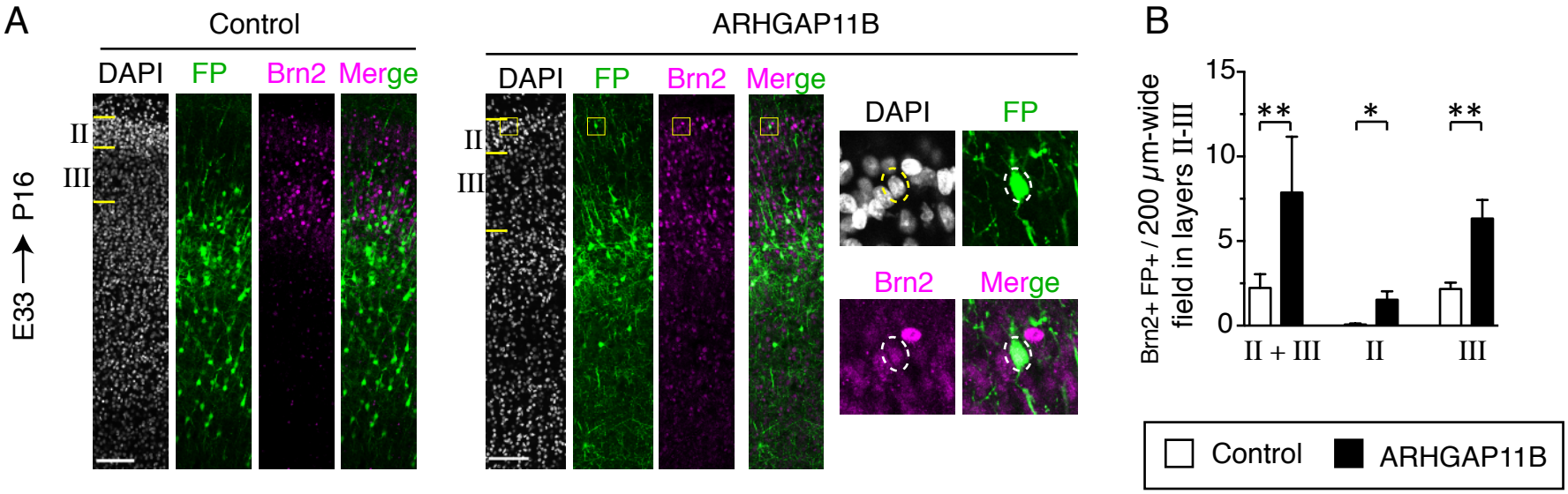

bioRxiv preprint doi: https://doi.org/10.1101/395830; this version posted August 20, 2018. The copyright holder for this preprint (which was not certified by peer review) is the author/funder. All rights reserved. No reuse allowed without permission.

Figure 4 supplement 3

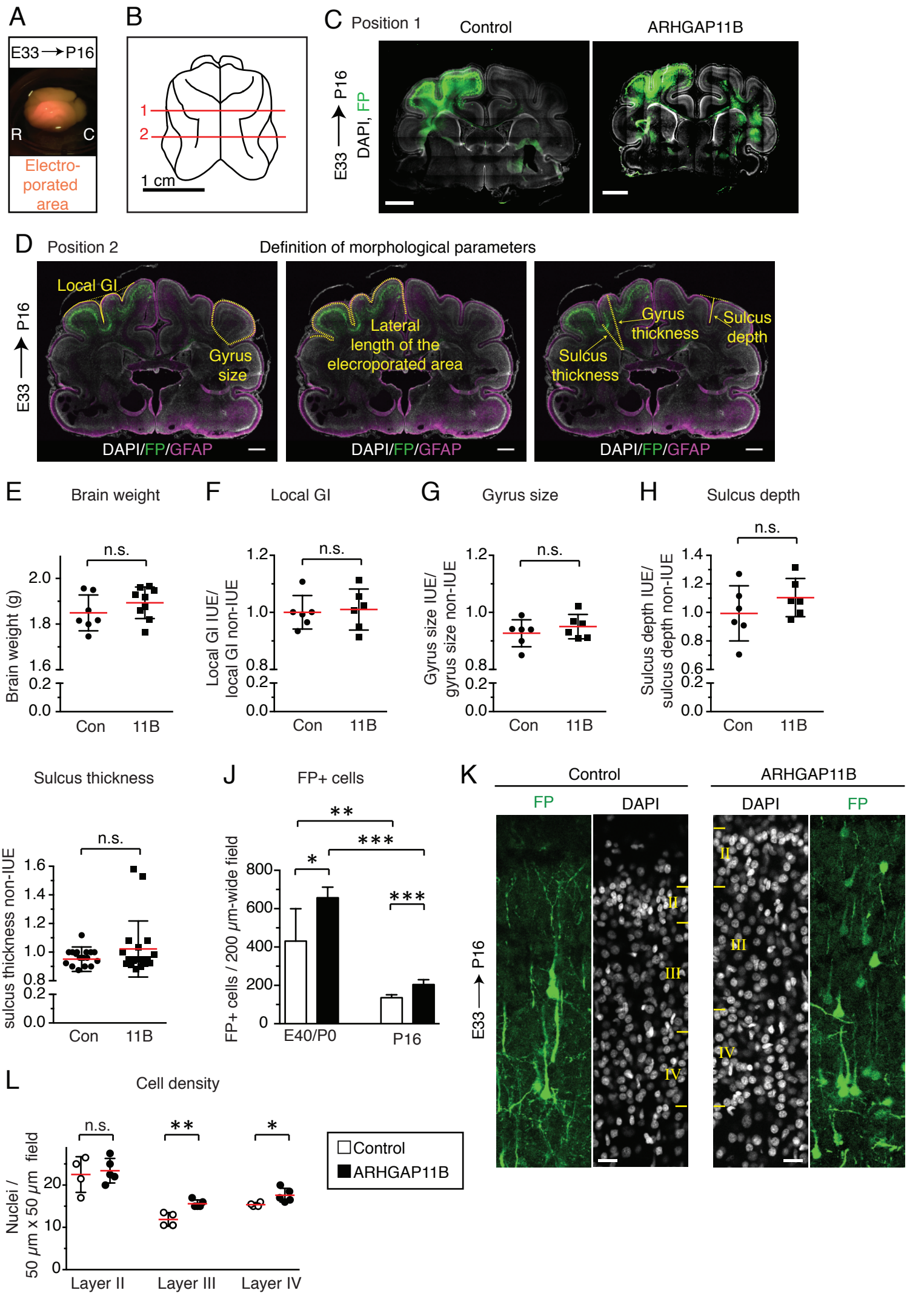

Figure 4 supplement 4

bioRxiv preprint doi: https://doi.org/10.1101/395830; this version posted August 20, 2018. The copyright holder for this preprint (which was not certified by peer review) is the author/funder. All rights reserved. No reuse allowed without permission.

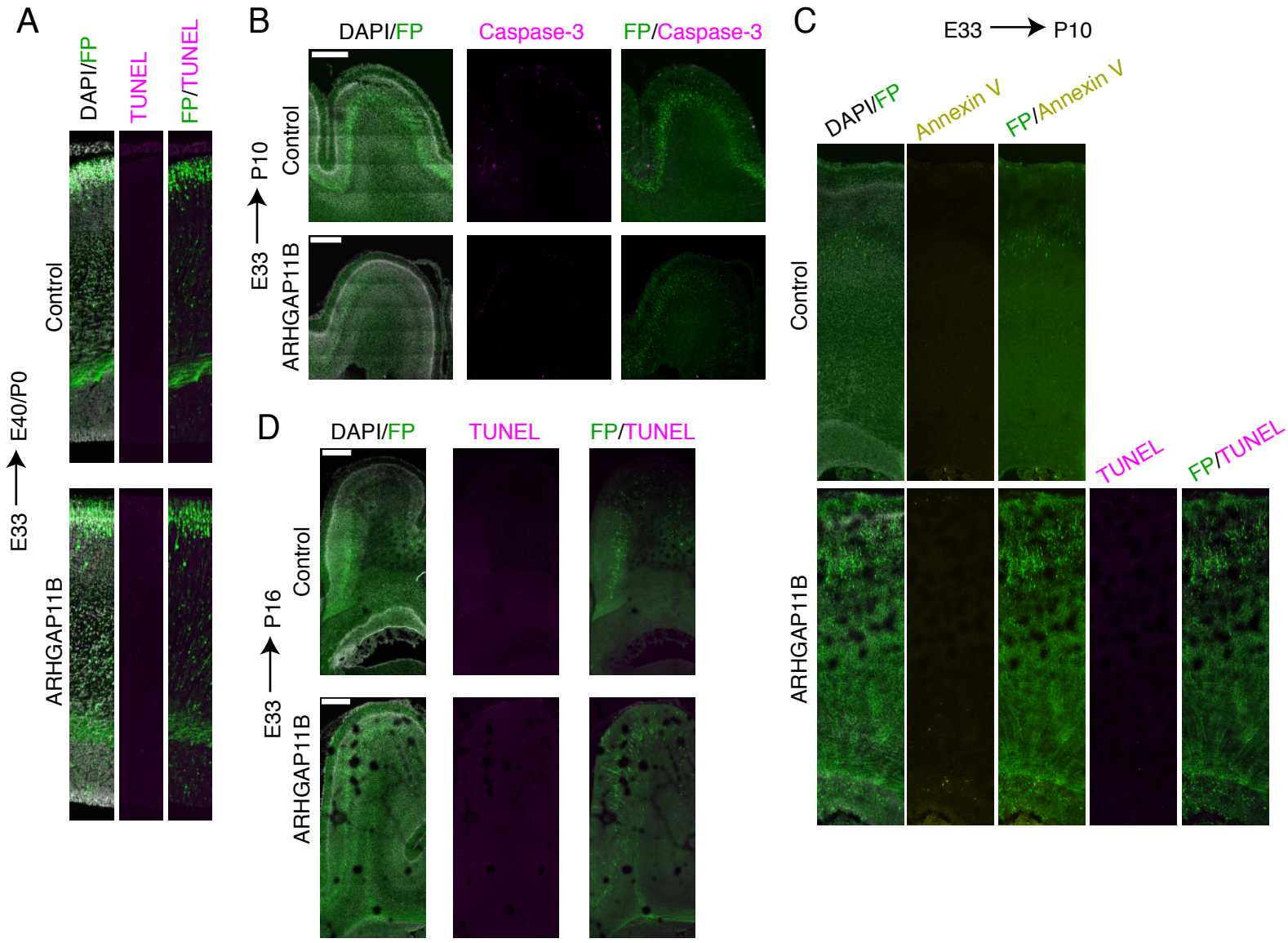

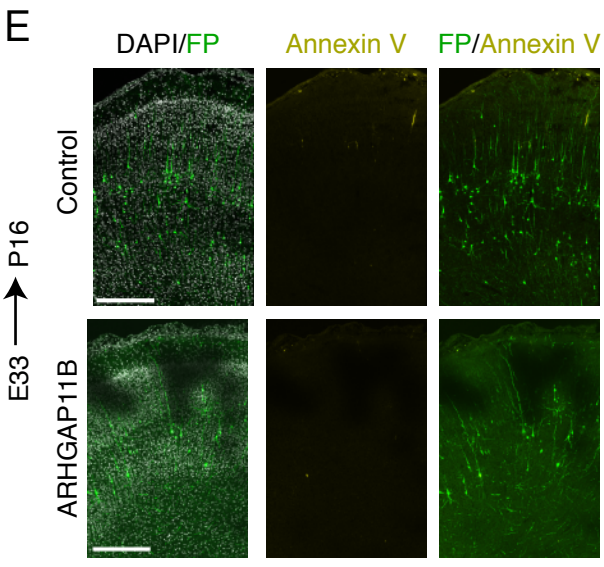

F

STAGE	APOPTOSIS DETECTION METHOD	CONDITION	APOPTOTIC FP+ / FP+ (%)
E40/P0	TUNEL	Control	<1%
		ARHGAP11B	<1%
P10	Caspase-3	Control	<1%
		ARHGAP11B	<1%
P10	Annexin V	Control	<1%
		ARHGAP11B	<1%
P10	TUNEL	ARHGAP11B	<2%
P16	Annexin V	Control	<1%
		ARHGAP11B	<1%
P16	TUNEL	Control	<2%
		ARHGAP11B	<1%

bioRxiv preprint doi: https://doi.org/10.1101/395830; this version posted August 20, 2018. The copyright holder for this preprint (which was not certified by peer review) is the author/funder. All rights reserved. No reuse allowed without permission.

Figure 4 supplement 5

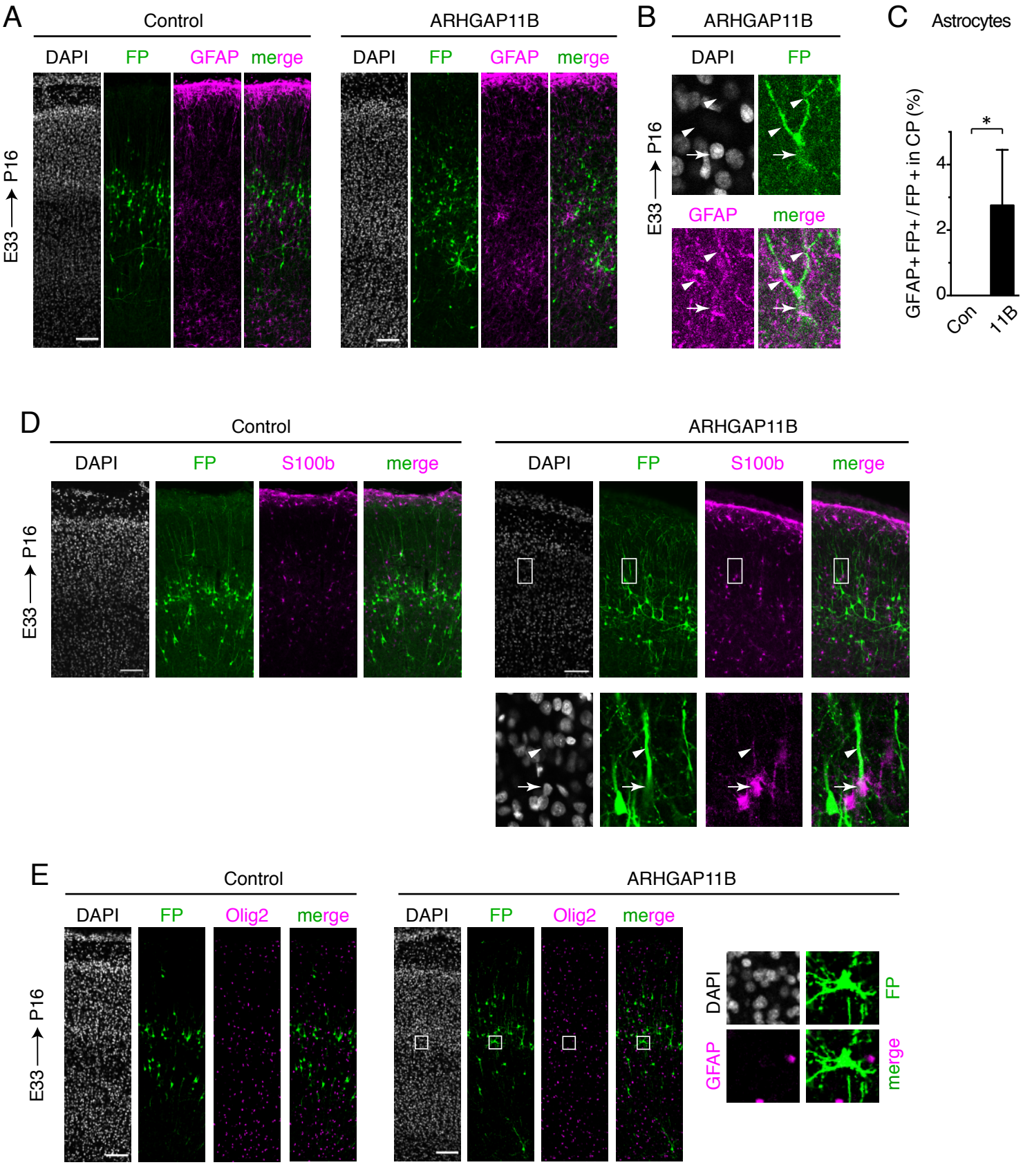

Supplemental Table 1. Overview of the effects of ARHGAP11B expression on neural progenitor cells and upper-layer neurons in developing ferret neocortex.

Cell type	Dev. stage			Data					ARHGAP11B vs. Control
NEURAL PROGENITOR CELLS	E40/P0	**PCNA**	OSVZ	PCNA+ FP+ cells (% of total FP+ in OSVZ)	FP+ cells / 200 μm-wide field in OSVZ	PCNA+ FP+ cells / 200 μm-wide field in OSVZ			**3.5**-fold increase
				(Figure 1C)	(data not shown)	(calculation)			
				Control 33% ARHGAP11B 52%	Control 161 ARHGAP11B 361	Control 53 ARHGAP11B 188			
		PhVim	SVZ			Mitotic bRG / 200 μm-wide field			**6.1**-fold increase
						(Figure 1F)			
						Control 0.375 ARHGAP11B 2.293			
UPPER-LAYER NEURONS	P16	**Satb2**	Layers II-IV	Satb2+ FP+ cells in layers II-IV (% of total FP+ in CP)	Satb2+ FP+ / 200 μm-wide field in CP	Satb2+ FP+ / 200 μm-wide field in layers II-IV	Relative lateral length of the FP+ area. Medio-lateral dimension. (Control set to 1)	Relative lateral length of the FP+ area. Rostro-caudal dimension. (Control set to 1)	**3.3**-fold increase *Calculations* *Control:* *43.3 x 1.0 x 1.0 =* ***43.3*** *ARHGAP11B:* *91 x 1.25 x 1.25 =* ***142.2***
				(Figure 4B)	(Figure 4 supplement 1C)	(calculation)	(Figure 4H)	(asumption)	
				Control 48.6% ARHGAP11B 71.1%	Control 89 ARHGAP11B 128	Control 43.3 ARHGAP11B 91	Control 1.0 ARHGAP11B 1.25	Control 1.0 ARHGAP11B 1.25	
		Brn2	Layers II-III			Brn2+ FP+ / 200 μm-wide field in layers II+III	Relative lateral length of the FP+ area. Medio-lateral dimension. (Control set to 1)	Relative lateral length of the FP+ area. Rostro-caudal dimension. (Control set to 1)	**5.6**-fold increase *Calculations* *Control:* *2.2 x 1.0 x 1.0 =* ***2.2*** *ARHGAP11B:* *7.9 x 1.25 x 1.25 =* ***12.3***
						(Figure 4 supplement 2B)	(Figure 4H)	(asumption)	
						Control 2.2 ARHGAP11B 7.9	Control 1.0 ARHGAP11B 1.25	Control 1.0 ARHGAP11B 1.25	